

Julia Kiri Ellinor Bådsvik

**NTNU**  
Norwegian University of  
Science and Technology  
Faculty of Engineering  
Department of Energy and Process Engineering

Julia Kiri Ellinor Bådsvik

# Development of a Francis Turbine Test Rig at Kathmandu University

February 2019





Norwegian University of  
Science and Technology

# Development of a Francis Turbine Test Rig at Kathmandu University

**Julia Kiri Ellinor Bådsvik**

Mechanical Engineering

Submission date: February 2019

Supervisor: Ole Gunnar Dahlhaug

Co-supervisor: Bjørn Winther Solemslie  
Biraj Singh Thapa  
Sailesh Chitrakar

Norwegian University of Science and Technology  
Department of Energy and Process Engineering



EPT-M-2018-122

**MASTER THESIS**for  
Julia Bådsvik

Autumn 2018

*Development of a Francis Turbine Test Rig at Kathmandu University*  
*Utvikling av en Francisturbin testrigg ved Kathmandu University***Background**

The Turbine Testing Laboratory at Kathmandu University was commissioned in 2011, and will be useful for future developments and improvements of hydraulic machinery necessary for the Nepali market and throughout the Himalaya region.

The laboratory is built up around a main pipe system, with the two main booster pumps located in the basement. Various running configurations are possible by utilizing different pipe loops, enabling both open and closed loop conditions. Kathmandu University are aiming to install test rigs equipped with high-precision measuring instruments in accordance with the IEC 60193 standard, enabling performance guarantee tests of Francis- and pump-turbines.

Recently, Kathmandu University received a grant from the Norwegian Government for a large research program named “EnergizeNepal” where one activity is aiming to build a state of the art Francis turbine test rig. NTNU will support the development of this test rig by giving technical support from the Waterpower Laboratory.

The Francis turbine test rig is being used for research and development tests, along with model acceptance tests. The tests comprise determination of performances, such as efficiency, discharge, head and power. The operating behaviors are investigated, such as cavitation behavior and operation at runaway. The dynamic phenomena such as pressure fluctuations, torques and forces will also be investigated.

**Objectives**

Design a calibration system for the flow rate measurement, axial load and friction torque measurements in the Turbine Testing Laboratory at Kathmandu University.

**The following tasks are to be considered:**

1. Literature study
  - Strain gauge measurements
2. Software knowledge
  - Labview
3. Manufacture and calibration
  - Axial load system for Kathmandu University
  - Friction torque system for Kathmandu University
4. Turbine Testing Laboratory, Kathmandu University
  - Make 3D-drawings for the main components of the calibration system.
  - Make a calibration procedure for the flow rate measurements
  - Make 3D-drawings for the axial load and friction torque system

Within 14 days of receiving the written text on the master thesis, the candidate shall submit a research plan for his project to the department.

When the thesis is evaluated, emphasis is put on processing of the results, and that they are presented in tabular and/or graphic form in a clear manner, and that they are analysed carefully.

The thesis should be formulated as a research report with summary both in English and Norwegian, conclusion, literature references, table of contents etc. During the preparation of the text, the candidate should make an effort to produce a well-structured and easily readable report. In order to ease the evaluation of the thesis, it is important that the cross-references are correct. In the making of the report, strong emphasis should be placed on both a thorough discussion of the results and an orderly presentation.

The candidate is requested to initiate and keep close contact with his/her academic supervisor(s) throughout the working period. The candidate must follow the rules and regulations of NTNU as well as passive directions given by the Department of Energy and Process Engineering.

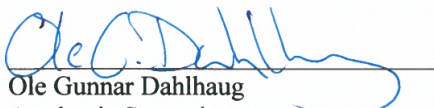
Risk assessment of the candidate's work shall be carried out according to the department's procedures. The risk assessment must be documented and included as part of the final report. Events related to the candidate's work adversely affecting the health, safety or security, must be documented and included as part of the final report. If the documentation on risk assessment represents a large number of pages, the full version is to be submitted electronically to the supervisor and an excerpt is included in the report.

Pursuant to “Regulations concerning the supplementary provisions to the technology study program/Master of Science” at NTNU §20, the Department reserves the permission to utilize all the results and data for teaching and research purposes as well as in future publications.

The final report is to be submitted digitally in INSPERA. An executive summary of the thesis including title, student's name, supervisor's name, year, department name, and NTNU's logo and name, shall be submitted to the department as a separate pdf file. Based on an agreement with the supervisor, the final report and other material and documents may be given to the supervisor in digital format.

- Work to be done in the Waterpower laboratory  
 Field work

Department of Energy and Process Engineering, 13. August 2018

  
Ole Gunnar Dahlhaug  
Academic Supervisor

Co-Supervisors:

- Bjørn Winther Solemslie
- Biraj Singh Thapa
- Sailesh Chitrakar

---

# Abstract

This Master's thesis is a part of the *EnergizeNepal* project, which aims to build a state-of-the-art Francis turbine test rig at Kathmandu University that fulfils the requirements of the IEC60193. Nepal has great hydroelectric power resources, where only a small percentage has been utilised. The main issue is that the high content of sediments in the water causes the turbines to erode. The purpose of building the laboratory is therefore to be able to test for these conditions and find effective solutions.

In this Master's thesis, a way of measuring and calibrating the axial force has been tested. The idea has been to place strain gauges at the lower section of the bearing block, a section named the Axial Load Measuring Device (ALMD), where the strain gauges will measure the strain caused by the axial force when the turbine is running. In order to achieve this goal, the axial force has been calculated theoretically, simulations have been set up in Ansys Mechanical and experiments in the Waterpower Laboratory at NTNU have been conducted.

The theoretical calculation gave a maximum axial force of  $7000N$ . Several scenarios using this maximum axial force and changing the wall thickness of the ALMD were run in Ansys Mechanical. It was found that when the ALMD had a wall thickness of  $1mm$ , the maximum stress seen in the model would be far below the yield strength.

The experiments were conducted at two wall thicknesses:  $2mm$  and  $18mm$ . By using a rig set up in the laboratory, an axial force could be applied to the ALMD. Loads between  $0kg - 200kg$  and  $500kg - 700kg$  were added  $20kg$  at a time. Because of lack of weights, there was a gap between  $200kg - 500kg$  where no measurements could be made.

It was found that both wall thicknesses gave large uncertainties for some of the loads. The highest uncertainty found was 36% and 15% for the  $2mm$  and  $18mm$  wall thicknesses respectively, both at a load of  $20kg$ . The uncertainty however decreases for higher loads, giving an uncertainty of 1% – 3% at a load of  $700kg$  for both cases. The greatest contributor to the uncertainty was the hysteresis, that was large, especially above  $500kg$ . On the other hand, the repeatability was good for both cases.

In order to use the ALMD as a measuring device, a calibration curve was made. A best fit curve was plotted between the data points, and it was found that the deviation between the modelled and the actual loads was high for the  $18mm$  wall thickness at some measuring points. The  $2mm$  wall thickness also gave some deviation, although much smaller. The strain gauges proved dependent on temperature, and a temperature compensation was therefore performed.

---

# Sammendrag

Denne masteroppgaven er en del av prosjektet *EnergizeNepal*, som har som mål å utvikle og bygge en francisturbin-testrigg for Universitetet i Kathmandu som oppfyller kravene i IEC60193. Nepal har store vannkraftressurser, men bare en liten andel er utbygd. Hovedproblemet er at det er høyt innhold av sedimenter i vannet slik at turbinene eroderer. Poenget med å bygge laboratoriet er derfor å kunne teste for slike forhold og finne gode løsninger.

I denne masteroppgaven er en metode for å måle og kalibrere aksialkraften testet. Ideen er å plassere strekkklapper på den nederste delen av lagerblokken, en seksjon som kalles Axial Load Measuring Device (ALMD), hvor strekkklappene vil måle strekk påført av aksialkraften når turbinen er i drift. For å oppnå dette, er aksialkraften regnet ut teoretisk, simuleringer er satt opp i Ansys Mechanical og eksperimenter er gjennomført på Vannkraftlaboratoriet ved NTNU.

Den teoretiske utregningen ga en maksimal aksialkraft på  $7000N$ . Flere scenarier der den maksimale aksialkraften og forskjellige ALMD-veggytkkelser ble benyttet, ble kjørt i Ansys Mechanical. Det ble funnet at ved en veggytkkelse på  $1mm$  ville den maksimale spenningen i modellen være langt under flytegrensen.

Eksperimentene ble utført for to veggytkkelser:  $2mm$  og  $18mm$ . Ved å bruke en rigg i laboratoriet kunne det settes en aksialkraft på ALMD-en. Vekter mellom  $0kg - 200kg$  og  $500kg - 700kg$  ble lagt på  $20kg$  av gangen. På grunn av manglende vekter var det et hull mellom  $200kg - 500kg$  hvor det ikke kunne foretas målinger.

Det ble funnet at begge veggytkkelsene ga store usikkerheter for noen av lastene. Den høyeste usikkerheten var  $36\%$  og  $15\%$  for henholdsvis  $2mm$  og  $18mm$  veggytkkelse, begge ved en pålagt last på  $20kg$ . Usikkerheten gikk derimot ned for høyere laster og ga en usikkerhet rundt  $1\% - 3\%$  for en last på  $700kg$  for begge veggytkkelsene. Det som bidro mest til usikkerheten, var hysteresen, som var stor, spesielt over  $500kg$ . Repeterbarheten var derimot bra.

For å kunne bruke ALMD-en som måleverktøy, ble det laget en kalibreringskurve. En best fit-kurve ble plottet mellom datapunktene, og det ble funnet at avviket mellom den modellerte og den faktiske lasten var stor for  $18mm$  veggytkkelse ved noen punkter.  $2mm$  veggytkkelse ga også noe avvik, men mye mindre. Strekkklappene viste seg å være avhengige av temperatur, og det ble derfor gjennomført en temperaturkompensering.



---

# Preface

This Master's thesis is written at the Department of Energy and Process Engineering at NTNU, in autumn 2018.

As a part of the *EnergizeNepal* project, this Master's thesis looks at developing an axial load measuring system to help the development of building a fully equipped turbine testing laboratory at Kathmandu University. This project has been very rewarding for me both because of the importance the laboratory will have for the development of hydroelectric power in Nepal, but also because of the many challenges I had to overcome and the new knowledge I have acquired. I am very grateful for having been given the opportunity to work on this project.

I would like to thank my supervisor, Prof. Ole Gunnar Dahlhaug, for all his help and guidance throughout this project, and for giving me opportunities I would not have gotten without him. Einar Agnalt also deserves a token of my appreciation for always answering my questions and being a good discussion partner. His guidance has been essential for the development of this thesis. I also owe a debt of gratitude to Joar Grilstad for helping me in the laboratory.

I would like to thank the people at TTL for being very welcoming when I visited, and for showing me around and keeping me entertained during my stay. I would also like to thank my fellow students at VKL for a fun semester, and to the staff for always being friendly and open for questions.

Last but not least, I would like to say a big thank you to my mom and dad, for always making my problems magically disappear.

---

# Table of Contents

<b>Abstract</b>	<b>i</b>
<b>Sammendrag</b>	<b>ii</b>
<b>Preface</b>	<b>iii</b>
<b>Table of Contents</b>	<b>vi</b>
<b>List of Tables</b>	<b>vii</b>
<b>List of Figures</b>	<b>x</b>
<b>Abbreviations</b>	<b>xi</b>
<b>Symbols</b>	<b>xii</b>
<b>1 Introduction</b>	<b>1</b>
1.1 Previous work . . . . .	2
1.2 The Francis Turbine Test Rig at NTNU . . . . .	3
1.3 The Turbine Testing Lab at Kathmandu University . . . . .	5
1.4 Objectives for the thesis . . . . .	6
<b>2 Theory</b>	<b>7</b>
2.1 Hydraulic similitude . . . . .	7
2.2 Strain gauges . . . . .	9
2.2.1 Measuring axial load with strain gauges . . . . .	10
2.3 Axial load computations . . . . .	11
2.3.1 Calculating the inlet and outlet pressure . . . . .	15
<b>3 Process</b>	<b>19</b>
3.1 Calculation of the axial forces in the turbine . . . . .	19
3.2 Simulations in Ansys Mechanical . . . . .	21

---

3.3	Experiments . . . . .	23
3.3.1	Calibration method . . . . .	26
<b>4</b>	<b>Results and discussion</b>	<b>29</b>
4.1	Numerical analysis . . . . .	29
4.2	Experiments . . . . .	32
4.2.1	Experiment 1, Temperature Compensation . . . . .	32
4.2.2	Experiment 1, Load Measurement . . . . .	35
4.2.3	Experiment 2, Load Measurement . . . . .	42
4.2.4	Comparing the experiments . . . . .	49
4.3	Comparing the experiments with the numerical analysis . . . . .	52
<b>5</b>	<b>Conclusion</b>	<b>53</b>
<b>6</b>	<b>Further work</b>	<b>55</b>
	<b>Appendix</b>	<b>58</b>
<b>A</b>	<b>Machine drawing of the ALMD</b>	<b>A1</b>
<b>B</b>	<b>Procedure for conducting temperature compensation with strain gauges</b>	<b>B1</b>
<b>C</b>	<b>Calibration procedure for the Axial Load Measuring Device</b>	<b>C1</b>

# List of Tables

3.1	Calculated axial forces for the BEP and maximum flow rate cases. . . . .	21
4.1	Results from the simulations in Ansys Mechanical when a force of $7000N$ is applied downwards. . . . .	30
4.2	Comparing the maximum stresses in different scenarios for $1mm$ and $2mm$ wall thickness. . . . .	30
4.3	Calculation of the errors in load step $F = 196.44N$ at a wall thickness of $2mm$ . . . . .	46
4.4	Comparing the simulations to the experiments for the $2mm$ wall thickness. . . . .	52
4.5	Comparing the simulations to the experiments for the $18mm$ wall thickness. . . . .	52

---

---

# List of Figures

1.1	Open loop, mode 8 at VKL. [12]	4
1.2	Closed loop, mode 5 at VKL. [12]	4
1.3	Outside view of TTL.	5
2.1	Sectional view of a Francis turbine. [14]	8
2.2	Elongation of an object when a force is applied. [17]	9
2.3	Wheatstone Bridge. [17]	10
2.4	Full bridge setup for measuring axial forces. [18]	11
2.5	Sectional view of the turbine and bearing block at TTL.	12
2.6	The axial forces working on a runner. [20]	13
2.7	Cross sectional view of the runner at TTL with dimensions.	14
2.8	Illustrative figure of the turbine and the lower reservoir.	15
2.9	Velocity triangle for the inlet of a runner. [21]	16
2.10	Velocity triangle for the outlet of a runner. [21]	17
2.11	Velocity triangle for the outlet of a runner at BEP. [21]	17
3.1	Full and sectional view of the TTL bearing block, showing the ALMD.	20
3.2	The middle section of the ALMD in Ansys Mechanical, coloured blue.	22
3.3	Mesh used for the ALMD in the simulations.	23
3.4	Test rig for the axial force measurements, also showing the placement of two of the strain gauges. The other two are 180° apart and therefore not visible in the diagram.	24
3.5	Experiment setup for loads below 200kg.	25
3.6	Measuring sequence recommended in the <i>DKD-R 6-1 Guideline</i> . [25]	25
3.7	Lever beam concept recommended by Selmurzaev for calibrating the axial load measuring system. [8]	26
3.8	Axial force calibration system. [8]	27
3.9	The axial force calibration system connected to the Francis turbine rig. [8]	27
4.1	Distribution of stress for the 2mm wall thickness.	31
4.2	Distribution of strain for the 2mm wall thickness.	31

---

4.3	Distribution of deformation for the 2mm wall thickness. . . . .	31
4.4	Temperature curves for the 18mm wall thickness. . . . .	32
4.5	Best fit line for the temperature curves for the 18mm wall thickness. . . . .	33
4.6	Temperature curves for the 18mm wall thickness after temperature correction has been done. . . . .	34
4.7	Axial load measurement for the 18mm wall thickness. . . . .	35
4.8	The two repetitions superimposed for the 18mm wall thickness. . . . .	36
4.9	Measuring points for the on-loading and off-loading for the 18mm wall thickness. The best fit curve is plotted between the data points. . . . .	37
4.10	Deviation between modelled and actual load for the 18mm wall thickness using a first order polynomial. . . . .	38
4.11	Deviation between modelled and actual load for the 18mm wall thickness using a second order polynomial. . . . .	38
4.12	The absolute range of error for the modelled loads at a wall thickness of 18mm. . . . .	40
4.13	The percentage range of error for the modelled loads at a wall thickness of 18mm. . . . .	40
4.14	The contribution from the hysteresis, repeatability and zero deviation to the total error for the 18mm wall thickness. . . . .	41
4.15	Axial load measurement for the 2mm wall thickness. . . . .	42
4.16	The two repetitions superimposed for the 2mm wall thickness. . . . .	43
4.17	Measuring points for the on-loading and off-loading for the 2mm wall thickness. The best fit curve is plotted between the data points. . . . .	44
4.18	Deviation between modelled and actual load for the 2mm wall thickness using a first order polynomial. . . . .	45
4.19	Deviation between modelled and actual load for the 2mm wall thickness using a second order polynomial. . . . .	45
4.20	The absolute range of error for the modelled loads at a wall thickness of 2mm. . . . .	47
4.21	The percentage range of error for the modelled loads at a wall thickness of 2mm. . . . .	47
4.22	The contribution from the hysteresis, repeatability and zero deviation to the total error for the 2mm wall thickness. . . . .	48
4.23	Deviation between the modelled and actual load for the 18mm and 2mm wall thicknesses. . . . .	51



---

# Abbreviations

<b>ALMD</b>	Axial Load Measuring Device
<b>BEP</b>	Best Efficiency Point
<b>DAQ</b>	Data Acquisition
<b>GF</b>	Gauge factor
<b>IEC</b>	International Electrotechnical Commission
<b>KU</b>	Kathmandu University
<b>mwc</b>	meters water column
<b>NPSH</b>	Net Positive Suction Head
<b>NORAD</b>	Norwegian Agency of Development Corporation
<b>NTNU</b>	Norwegian University of Science and Technology
<b>SG</b>	Strain gauge
<b>TTL</b>	Turbine Testing Lab
<b>VKL</b>	Waterpower Laboratory

---

# Symbols

Symbol	Definition	Unit
$A$	Area	$m$
$c$	Absolute velocity	$m/s$
$D$	Diameter	$m$
$E$	Young's modulus	$N/m^2$
$F$	Force	$N$
$g$	Gravitational acceleration	$m/s^2$
$h$	Pressure	$mwc$
$H_n$	Net head	$m$
$k$	Constant	—
$L$	Length	$m$
$n_{ED}$	Speed factor	—
$p$	Pressure	$Pa$
$Q$	Flow rate	$m^3/s$
$Q_{ED}$	Discharge factor	—
$R$	Resistance	$\Omega$
$T$	Temperature	$^{\circ}C$
$u$	Tangential velocity	$m/s$
$V$	Voltage	$V$
$z$	Height	$m$
$\beta$	Outlet blade angle	$^{\circ}$
$\epsilon$	Strain	$mm/mm$
$\eta_h$	Hydraulic efficiency	—
$\rho$	Density	$kg/m^3$
$\sigma$	Stress	$MPa$
$\sigma_T$	Thoma number	—
$\phi$	Angle of velocity	$^{\circ}$
$\omega$	Angular velocity	$rad/s$
$b'$	Repeatability	—
$f_0$	Zero deviation	—
$h$	Hysteresis	—
$M_{iw}$	Mean value	—
$U_{total}$	Uncertainty	—

# Introduction

Nepal is a mountainous country considered to be one of the poorest countries in the world [1]. It is landlocked between the two major countries, China in the north and India in the south. Along its northern border the Himalaya range rises, being the home of some of the highest peaks in the world. During the summer, the glaciers and snow melt, giving the country a great potential for hydroelectric power. However, only a small percentage of this energy has been utilised. [2]

The way of living is still very primitive in Nepal. Fire wood and agricultural waste are used for energy, cooking and heating, creating pollutants and an unhealthy indoors environment. The country has no known deposits of coal, oil or gas and is therefore dependent on importing fuel from its neighbouring country India. Some electricity is also imported from India. A hope is therefore that if more hydroelectric power is developed, the country can be self-sufficient in energy, and maybe also sell surplus power to its neighbours, getting the country out of its poverty. [2]

The main issue with hydroelectric power in Nepal is that there is a lot of sediment in the water that erodes the turbines. The turbines therefore have a short life span before they have to be taken out and refurbished. In order to make hydroelectric power more economically viable, turbines that can withstand greater erosion should be developed. It is for this reason that Kathmandu University (KU) wants to build a waterpower laboratory.

Waterpower laboratories can be found several places in the world. Most turbine manufacturers have them, and also a handful of universities. The purpose of a waterpower laboratory is to test model turbines for the same conditions as the prototype is exposed to, and find a design that is best suited to the local conditions. Another important purpose for a waterpower laboratory is to develop and build competence and knowledge within the waterpower sector. Both these approaches will give more confidence in the final product. [3]

In 1997, it was therefore decided that a waterpower laboratory would be developed at KU. In 2009, KU signed an agreement with the Norwegian Agency for Development Corporation (NORAD), where NORAD agreed to help finance the building of the Turbine Testing Lab (TTL). The Norwegian University of Science and Technology (NTNU) is helping this process by giving technical support from the NTNU Waterpower Laboratory (VKL). [4]

This Master's thesis is a part of the *EnergizeNepal* project, where the aim is to build a state-of-the-art Francis turbine test rig at KU that fulfils the requirements of the IEC60193 standard. Several Master's theses have earlier been written for this project, helping the development of the project.

## 1.1 Previous work

In 2012, Bidhan Halwai made a design of the Francis runner at TTL based on the Francis runner at Jhimruk Hydroelectric Power Plant in Nepal [5]. A 3D model of the test rig was made and was put into the drawings of the pipe system at TTL. Later, changes were made to his design by the engineers at TTL.

Johanne Seierstad made a suggestion for calibrating the flowmeter in her Master's thesis in 2013 [6]. She suggested using the volumetric method and made suggestions for the placement of the flowmeter and also made cost estimations for her system. When Inger Johanne Rasmussen designed TTL in her Master's thesis, she used Seierstad's flow rate calibration system. She also designed the high pressure tank, the low pressure tank, the guide vane control system, the main shaft and bearing block. She also made suggestions for the measuring equipment for the laboratory and its placement. [7]

In 2016, Magomed Selmurzeav made a system to measure the axial force and friction torque using strain gauges [8]. He also made a system to calibrate both these parameters and made 3D models of the system. Morten Grefstad used this system when he made a measuring system for the axial load in 2017, where he also made 3D drawings of the main components of the laboratory at KU [9]. At the same time as Grefstad was writing his Master's thesis, Andreas Kjerschow wrote his Master's thesis on handling and processing the signals of the Francis turbine test rig, where he made a logging program in LabVIEW for TTL [10].

The author of this Master's thesis also wrote a Project thesis in the spring of 2018 where she designed a calibration system for the flow rate measurements [11]. 3D drawings of the weighing tank were made and were put into the previously made 3D drawings of the laboratory.

## 1.2 The Francis Turbine Test Rig at NTNU

The Turbine Testing Lab at Kathmandu University is based on the design of the Water-power Laboratory (VKL) at NTNU, and understanding how VKL is designed and operated is therefore important. This section and Section 1.3 are copied from the author's Project thesis [11].

In the basement of VKL are located two pumps rated at  $287.1kW$  with the possibility of running the pumps in series, parallel or individually. It is also possible to change the rotational speed of the pumps. By making these changes a variation in flow and head can be achieved, with a highest possible pressure of  $100mwc$  when the pumps run in series.

VKL has two setups for running the Francis turbine test rig; in an open loop or in a closed loop. When running in an open loop, the water will be pumped from the water reservoir underneath the building (the sump), through the laboratory setup and directed back to the sump. An example of an open loop is mode 8 shown in Figure 1.1. Here the water is pumped to the upper reservoir. The upper reservoir is placed on the 5th floor and is shaped like a U. The water runs around the U-shape open to the atmosphere and flows down through the high-pressure tank, into the Francis turbine, through the low-pressure tank and back into the sump.

When the test rig is run in a closed loop, the sump inlet valves are closed, and the water is instead directed back through the pump(s). The water is then pumped through the system again and this cycle is repeated. An example of a closed loop is mode 5, shown in Figure 1.2. The water is pumped to the high-pressure tank using one pump, runs through the Francis turbine, into the low-pressure tank and returns through the pipework back to the pump where the cycle is repeated. [12]

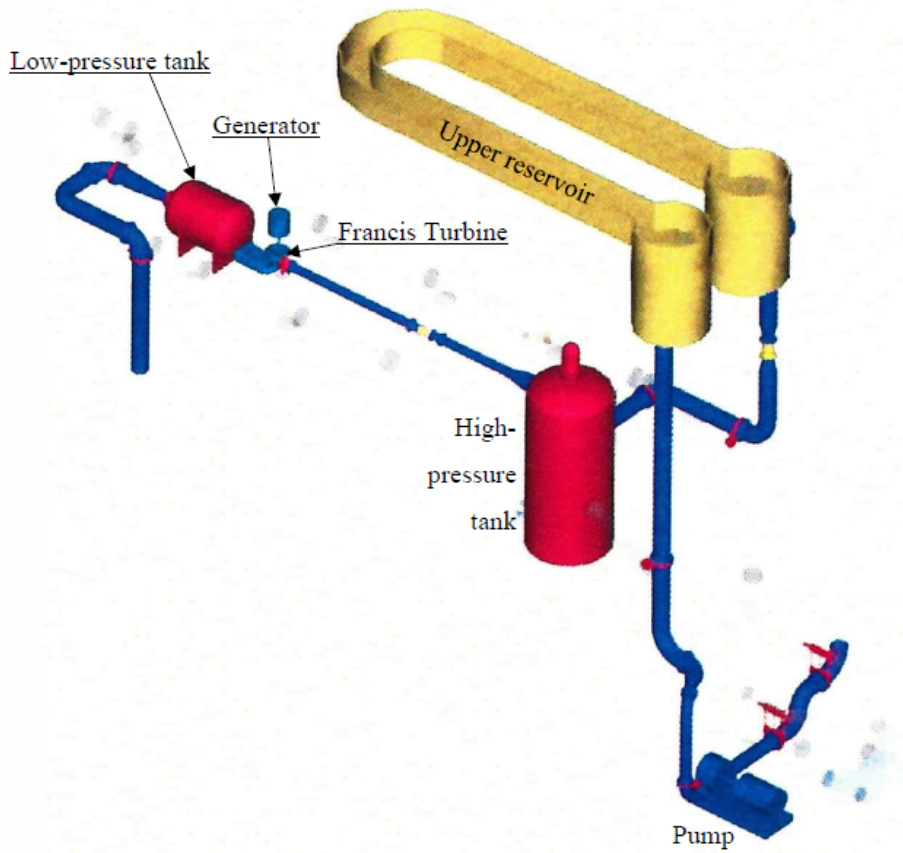


**Figure 1.1:** Open loop, mode 8 at VKL. [12]

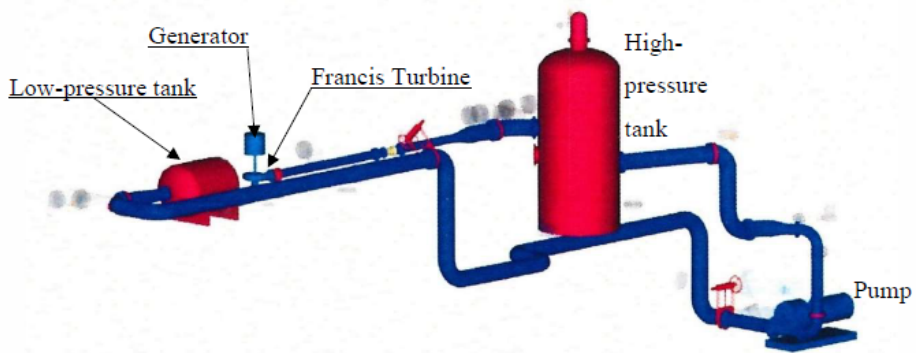


**Figure 1.2:** Closed loop, mode 5 at VKL. [12]

### 1.3 The Turbine Testing Lab at Kathmandu University

TTL is designed similarly to VKL. It has two pumps which can be run in series, parallel or individually, where each pump is of  $250kW$  rated capacity with the possibility to produce a maximum flow of  $0.5m^3/s$  and a maximum head of  $150m$ . The laboratory has an upper reservoir with the capacity to hold  $100m^3$  at the top of the campus, giving it a natural head of  $30m$ . Underneath the laboratory there is a reservoir with a capacity to hold  $300m^3$ . The laboratory will have the possibility to run in both an open and a closed loop, just like VKL. Figure 1.3 shows the outside of TTL with the upper reservoir. [4]

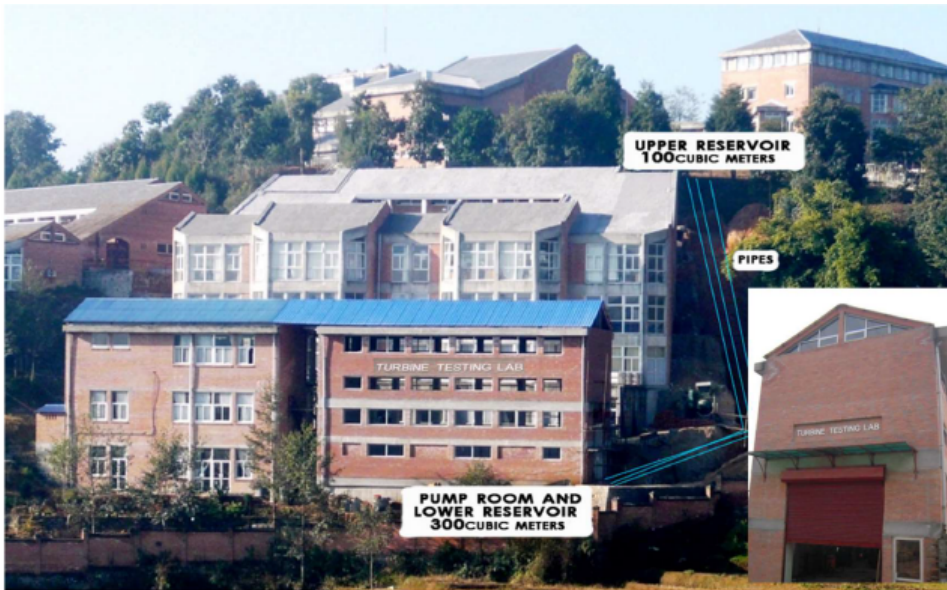


Figure 1.3: Outside view of TTL.

## 1.4 Objectives for the thesis

The objectives for this thesis are: *Design a calibration system for the flow rate measurement, axial load and friction torque measurements in the Turbine Testing Lab at Kathmandu University.*

It was early on decided that the main focus of this Master's thesis would be to test and calibrate the axial force and friction torque. A new system where strain gauges would be mounted on the lower section of the bearing block was to be tested in the laboratory. However, manufacturing and building the rig and bearing block section, and doing experiments to determine how to measure the axial force, proved time consuming. For this reason, there was not enough time to do any tests for the friction torque.

It was also decided that the work done in the author's Project thesis [11] on the flow calibration system was sufficient for the development of TTL. Further work was therefore not conducted on this topic.

This Master's thesis therefore aims to design an axial force measuring system and a way of calibrating it. The main focus has been to do tests in the laboratory with the aim of making the uncertainty small enough to create a good measuring system.



# Theory

This section and Section 2.1 are loosely copied from the author's Project thesis [11].

There are three main turbines used in hydroelectric power production, the Francis, Kaplan and Pelton turbines. The Francis turbine is however the most widely used as it has a broad range of applications. It can be used for heads up to  $750m$  and has a better peak efficiency than the other turbine designs.

The Francis turbine is a reaction turbine, meaning that it is driven by the difference in pressure between the inlet and outlet. Mechanical energy is produced partially from the pressure drop through the runner and partially from the impulse forces due to the relative velocity vectors changing direction. The drop in pressure can only be achieved if the turbine is completely submerged in water.

The turbine works by water flowing into the spiral casing where it is led through the static stay vanes and the movable guide vanes into the runner. The cross sectional area of the spiral casing is gradually narrowed to keep the flow accelerating and also cause the flow to rotate. The guide vanes can be regulated in order to get the flow to enter the runner at the desired angle of attack and to regulate the flow rate. The flow then goes through the runner where the mechanical energy is produced before escaping through the draft tube with reduced rotation and pressure. The draft tube broadens out with an increasing cross section to avoid cavitation in the turbine. Figure 2.1 shows a cross section of a Francis turbine. [13]

## 2.1 Hydraulic similitude

As doing performance tests on a full size turbine (prototype) is costly and impractical, tests are done on model turbines instead. In order to do these tests, the prototype and the model turbine need to be hydraulically similar. According to the IEC60193 standard [15], hydraulic similitude is achieved if the model and prototype turbines are geometrically similar and the forces acting between the machine components and the fluid have the same ratios. The ratios are Euler ( $Eu = \frac{\text{pressure}}{\text{inertia}}$ ), Reynolds ( $Re = \frac{\text{inertia}}{\text{viscosity}}$ ), Weber

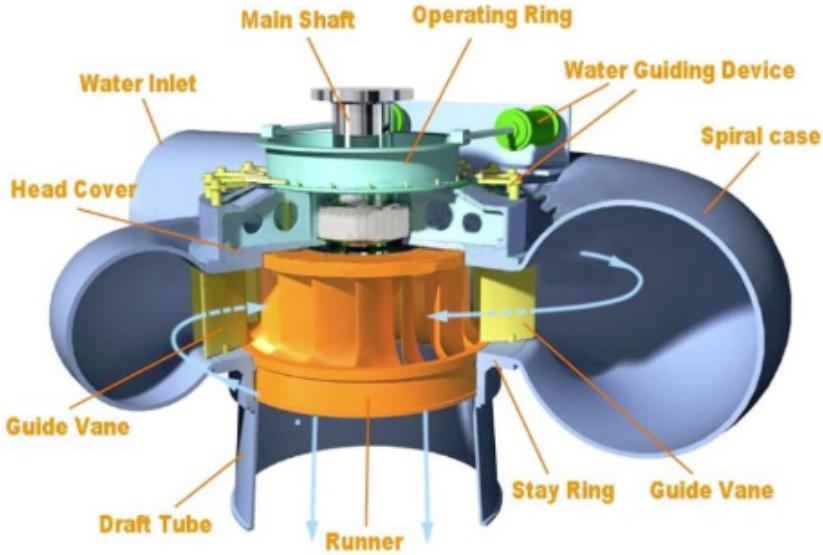


**Figure 2.1:** Sectional view of a Francis turbine. [14]

( $We = \frac{\text{inertia}}{\text{surface tension}}$ ) and Froude ( $Fr = \frac{\text{inertia}}{\text{gravity}}$ ). To achieve test conditions that satisfy all these ratios at the same time, is usually impossible. Hydraulic similitude is therefore considered to be achieved if the model and prototype have the same discharge factor ( $Q_{ED}$ ), speed factor ( $n_{ED}$ ) and Thoma number ( $\sigma_T$ ), as seen in equations (2.1), (2.2) and (2.3) respectively.

$$(Q_{ED})_{prototype} = (Q_{ED})_{model} = \frac{Q}{D_o^2 \sqrt{gH_n}} \quad (2.1)$$

$$(n_{ED})_{prototype} = (n_{ED})_{model} = \frac{nD_o}{60\sqrt{gH_n}} \quad (2.2)$$

$$(\sigma_T)_{prototype} = (\sigma_T)_{model} = \frac{NPSH}{H_n} \quad (2.3)$$

Here  $Q$  is the flow rate,  $D_o$  is the outlet diameter of the turbine,  $n$  is the rotational speed,  $H_n$  is the model net head,  $g$  is the gravitational acceleration and  $NPSH$  is the Net Positive Suction Head.

## 2.2 Strain gauges

Strain is defined as the elongation or compression of a section of material and is often due to a force or a change in temperature. Strain follows Hooke's law which means that the deformation is proportional to the force applied. Equation (2.4) gives the equation for strain. [16]

$$\varepsilon = \frac{\Delta L}{L} = \frac{F}{EA} \quad (2.4)$$

Here  $\varepsilon$  is the strain,  $L$  is the initial length and  $\Delta L$  is the difference in length from the initial state to the state where force is applied,  $F$  is the force applied,  $E$  is Young's modulus and  $A$  is the area. Figure 2.2 illustrates the definitions of change in length when a force is applied.

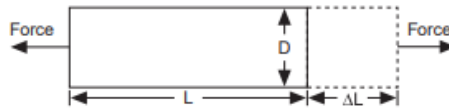


**Figure 2.2:** Elongation of an object when a force is applied. [17]

Strain gauges are used to measure the strain of an object and are put on the object where the strain is assumed to be high. Strain gauges measure the strain by measuring the change in electrical resistance as the object is elongated or compressed. The resistance measured is proportional to the strain in the object as the resistance increases when the strain gauge is stretched and decreases when it is compressed.

The gauge factor (GF) is an important parameter as it is the strain gauge's sensitivity to strain. The gauge factor is given by equation (2.5), where  $R$  is the initial resistance measured and  $\Delta R$  is the change in resistance measured. The gauge factor will always be quoted by the manufacturer.

$$GF = \frac{\Delta R/R}{\Delta L/L} = \frac{\Delta R/R}{\varepsilon} \quad (2.5)$$

The strain measured is usually very small. It is also important to be aware that strain gauges are very sensitive to change in temperature and for these two reasons strain gauges are often set up in a bridge configuration such as the Wheatstone bridge shown in Figure 2.3. The Wheatstone bridge has four resistances and a voltage or current source. The voltage output ( $V_0$ ) is given by equation (2.6)

$$V_0 = \left[ \frac{R_3}{R_3 + R_4} - \frac{R_2}{R_1 + R_2} \right] \cdot V_{EX} \quad (2.6)$$

where  $V_{EX}$  is the excitation voltage and  $R_1$ ,  $R_2$ ,  $R_3$  and  $R_4$  are the resistances for the different resistors.

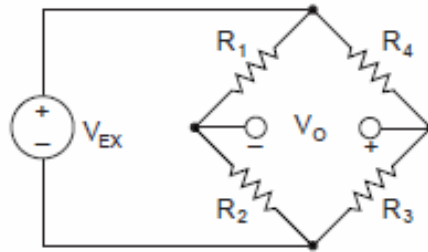


**Figure 2.3:** Wheatstone Bridge. [17]

$V_0$  will be zero if the bridge is balanced. This happens when either 1 or 2 occurs:

1.

$$R_1 = R_2 = R_3 = R_4$$

2.

$$\frac{R_1}{R_2} = \frac{R_4}{R_3}$$

In order to measure the strain, the voltage output cannot be zero. Instead, at least one of the resistors is replaced by a strain gauge. Depending on how many resistors are replaced, the Wheatstone bridge is described variously as a quarter bridge, half bridge or full bridge, where one, two or four strain gauges are inserted respectively. Because a full bridge uses four strain gauges, it gives a four times stronger signal than a quarter bridge.

### 2.2.1 Measuring axial load with strain gauges

To measure the axial load with strain gauges, the strain gauges should be placed in a bridge configuration as seen in Figure 2.4. SG1 and SG3 are the active strain gauges, measuring the difference in strain at different axial loads, and SG2 and SG4 are dummy strain gauges. The purpose of the dummy strain gauges is to compensate for temperature. All four strain gauges will be affected equally by the change in temperature and they will therefore cancel out temperature effects. The output from the bridge should then only be due to the change in axial load.

The measured strain using a full bridge is calculated using equation (2.7).

$$\epsilon = \frac{V_0}{V_{EX}} \frac{1}{GF} \quad (2.7)$$

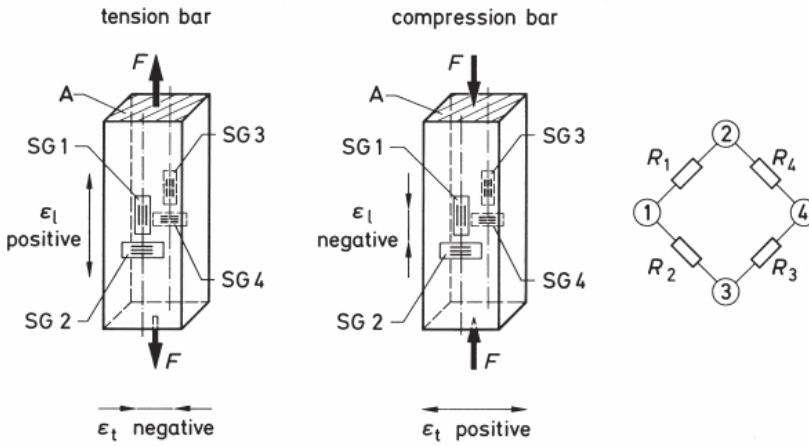


Figure 2.4: Full bridge setup for measuring axial forces. [18]

## 2.3 Axial load computations

An axial force results in the Francis turbine when it is running, which is caused by changes in pressure and direction of the absolute velocity. It is important to measure the axial force to design a sufficiently strong axial bearing. The axial force should always point downwards and should not exceed the force the bearing is designed for. Figure 2.5 shows a cross sectional view of the turbine and bearing block at TTL, with the axial force shown.

This section describes how the axial force is calculated, and is based on *Pumper & Turbiner* by Hermod Brekke [19]. The axial force is the sum of seven forces occurring in the runner, shown in Figure 2.6. The following assumptions have been made in order to do the calculations.

1. The flow is steady
2. The flow is incompressible
3. The flow is inviscid
4. Continuity is assumed

$F_1$  is the force due to the difference in the diameters of the hub and the shroud and is a pressure force as seen in equation (2.8). Here the subscripts 11 and 12 refer to the hub and the shroud respectively and the pressure distribution over the shroud area is approximated as  $\frac{1}{2}(h_{11} + h_{12})$ . Figure 2.7 shows the definitions and dimensions used in this section.

$$F_1 = p_1 A_1 = \frac{1}{2} \rho g (h_{11} + h_{12}) \frac{\pi}{4} (D_{12}^2 - D_{11}^2) \quad (2.8)$$

Here,  $p$  is the pressure,  $A$  is the area,  $\rho$  is the density of water,  $g$  is the gravitational acceleration and  $h$  is the pressure in meters water column (*mwc*). The subscript 1 means position 1, which is at the inlet of the runner.

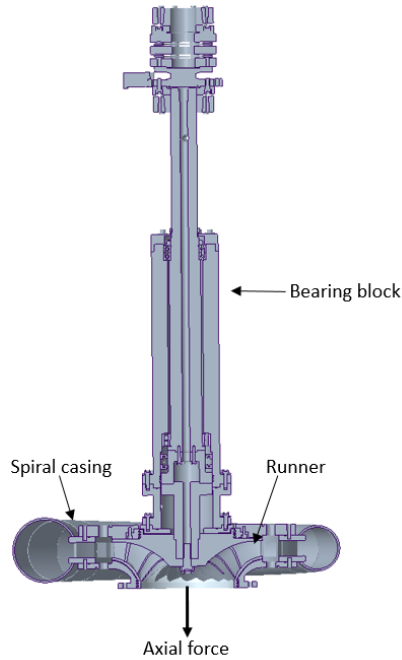


**Figure 2.5:** Sectional view of the turbine and bearing block at TTL.

$F_2$  is the reaction force in the turbine due to the change in direction of the absolute velocities and is the sum of the reaction forces at the runner inlet and runner outlet. The expression for  $F_2$  is given in equation (2.9).

$$F_2 = \rho Q(c_{m2} - c_{m1} \cdot \sin(\phi)) \quad (2.9)$$

where  $Q$  is the flow rate,  $\phi$  is the angle of the velocity when it enters the runner and  $c_{m1}$  and  $c_{m2}$  are the meridional velocities at the inlet and outlet respectively.

The meridional velocities are given by equation (2.10)

$$c_m = \frac{Q}{A} \quad (2.10)$$

where the area  $A$  is the area at the inlet and outlet of the runner for  $c_{1m}$  and  $c_{2m}$  respectively.

$F_3$  is the force caused by the outlet pressure and is given in equation (2.11).

$$F_3 = \rho g h_2 \cdot \frac{\pi D_{2L}^2}{4} \quad (2.11)$$

Here, the subscript 2 means the outlet of the runner and  $2L$  means the lower labyrinth seal.

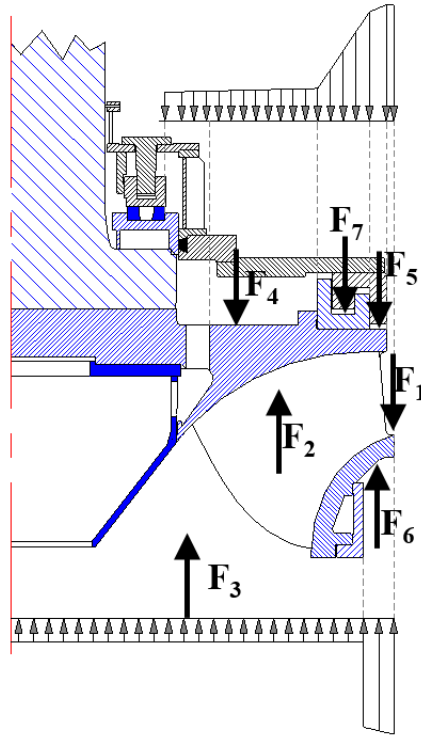


**Figure 2.6:** The axial forces working on a runner. [20]

$F_4$  is the force caused by the pressure between the runner hub and the top cover at the labyrinth seal low pressure side. It is given in equation (2.12)

$$F_4 = \rho g \left( \frac{h_p + h_s}{2} \right) \cdot \pi \cdot \left( \frac{D_p^2 - D_s^2}{4} \right) \quad (2.12)$$

where the subscript  $p$  means the low pressure side of the labyrinth and the subscript  $s$  refers to the shaft.

$F_5$  is the force caused by the pressure between the runner hub and the top cover at the labyrinth seal high pressure side and is given by equation (2.13).

$$F_5 = \frac{\rho \pi g h_{11}}{4} (D_{11}^2 - D_{11L}^2) - \frac{\rho \pi k^2 \omega^2}{64} (D_{11}^2 - D_{11L}^2)^2 \quad (2.13)$$

Here,  $k$  is a constant of value 0.5,  $\omega$  is the angular velocity and the subscript  $11L$  is the low pressure side on the upper labyrinth sealing.

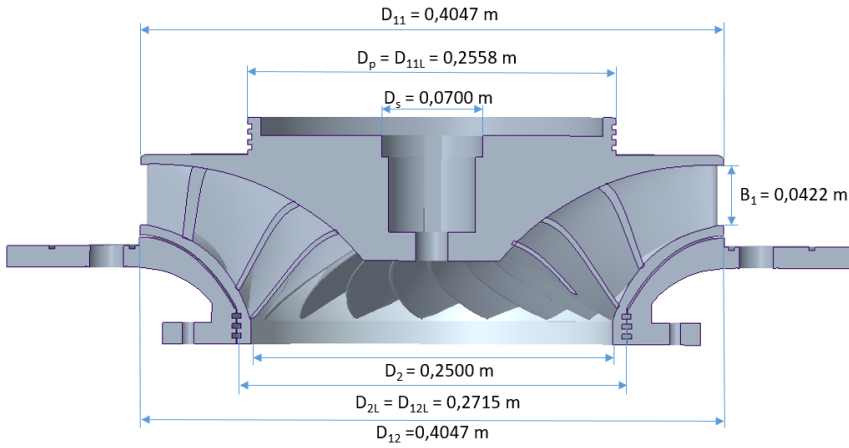


**Figure 2.7:** Cross sectional view of the runner at TTL with dimensions.

$F_6$  is the force caused by the pressure between the shroud and the lower cover on the labyrinth seal high pressure side and is given by equation (2.14).

$$F_6 = \frac{\rho\pi gh_{12}}{4} (D_{12}^2 - D_{12L}^2) - \frac{\rho\pi k^2 \omega^2}{64} (D_{12}^2 - D_{12L}^2)^2 \quad (2.14)$$

Subscript 12L is the low pressure side on the lower labyrinth sealing.

$F_7$  is the force caused by the upper labyrinth seal pressure and is given in equation (2.15).

$$F_7 = p_7 A_7 = \rho g \frac{h_{11L} + h_p}{2} \cdot \pi \cdot \frac{D_{11L}^2 - D_p^2}{4} \quad (2.15)$$

The total axial force is then given by equation (2.16) and is defined as positive when it is directed downwards.

$$F_{axial} = F_1 - F_2 - F_3 + F_4 + F_5 - F_6 + F_7 \quad (2.16)$$



### 2.3.1 Calculating the inlet and outlet pressure

To calculate the inlet and outlet pressure for the turbine, Bernoulli's equation is used. Figure 2.8 shows the defined points 1, 2 and 3, where point 1 is the inlet, point 2 is the outlet and point 3 is the lower reservoir. From the figure it can be seen that all the three points are at the same height, meaning that  $z_1 = z_2 = z_3$ . The height can therefore be disregarded in the Bernoulli equation.

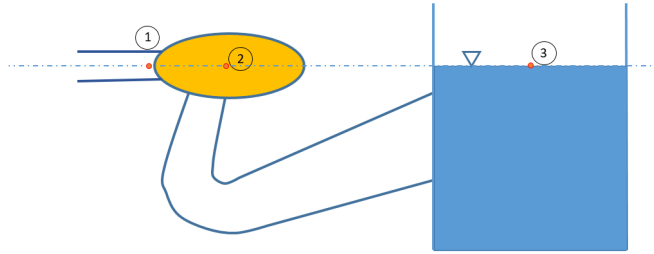


**Figure 2.8:** Illustrative figure of the turbine and the lower reservoir.

The only known pressure is the pressure at the lower reservoir, which is atmospheric. The pressure at the outlet ( $h_2$ ) can be found using Bernoulli's equation between points 2 and 3, and is given in equation (2.17). Here  $c$  is the absolute velocity and  $z$  is the nominal height. The velocity at the lower reservoir is assumed to be zero, meaning that  $c_3 = 0$ . As it is already known that  $z_2 = z_3$  and  $h_3 = h_{atm}$ , equation (2.17) simplifies to equation (2.18).

$$h_2 + \frac{c_2^2}{2g} + z_2 = h_3 + \frac{c_3^2}{2g} + z_3 \quad (2.17)$$

$$h_2 = h_{atm} - \frac{c_2^2}{2g} \quad (2.18)$$

Finding an expression for  $h_1$  is done similarly as for  $h_2$ , by using Bernoulli's equation between points 1 and 2. Equation (2.19) gives the expression for  $h_1$ , where  $H_n$  is the net head.

$$h_1 + \frac{c_1^2}{2g} + z_1 = h_2 + \frac{c_2^2}{2g} + z_2 + H_n \rightarrow h_1 = h_2 + \frac{1}{2g}(c_2^2 - c_1^2) + H_n \quad (2.19)$$

In order to solve the expressions for  $h_1$  and  $h_2$ , the absolute velocities  $c_1$  and  $c_2$  need to be calculated. They are calculated using the velocity triangles for the inlet and outlet of the runner. Figure 2.9 shows the velocity triangle for the inlet, and an expression for  $c_1$  can then be found, as given in equation (2.20).

$$c_1 = \sqrt{c_{m1}^2 + c_{u1}^2} \quad (2.20)$$

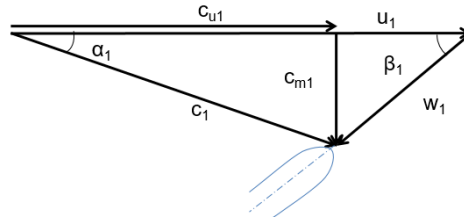


**Figure 2.9:** Velocity triangle for the inlet of a runner. [21]

The meridional velocity ( $c_m$ ) is calculated using equation (2.10). The cross-sectional area of the inlet is given in equation (2.21), where  $B_1$  is the height of the inlet.

$$A_1 = \pi D_1 B_1 \quad (2.21)$$

The component of the absolute velocity in the peripheral direction for the inlet ( $c_{u1}$ ) is found using Euler's turbine equation as seen in equation (2.22), where  $u$  is the absolute velocity in the peripheral direction. Turbines are designed so that the component of absolute velocity in the peripheral direction at the outlet ( $c_{u2}$ ) is zero at the best efficiency point (BEP) as zero rotation in the outlet is desirable. Equation (2.22) therefore simplifies to equation (2.23) at BEP. Continuity is assumed for all other operating points and the hydraulic efficiency ( $\eta_h$ ) is therefore assumed constant. Equation (2.23) therefore applies for every operating point for the turbine, not just BEP.

$$\eta_h = \frac{(u_1 c_{u1} - u_2 c_{u2})}{gH_n} \quad (2.22)$$

$$\eta_h = \frac{u_1 c_{u1}}{gH_n} \quad (2.23)$$

For hydropower turbines,  $\eta_h$  is assumed to be 96% and an expression for  $c_{u1}$  is then given in equation (2.24).

$$c_{u1} = \frac{\eta_h gH_n}{u_1} = \frac{0.96 \cdot gH_n}{u_1} \quad (2.24)$$

Finding an expression for  $c_2$  is done similarly as the calculations for  $c_1$  by using the velocity triangle for the outlet, seen in Figure 2.10, and is given in equation (2.25).

$$c_2 = \sqrt{c_{m2}^2 + c_{u2}^2} \quad (2.25)$$

$c_{m2}$  is calculated as  $c_{m1}$ , using equation (2.10), where the cross-sectional area is given by equation (2.26).

$$A_2 = \frac{\pi D_2^2}{4} \quad (2.26)$$

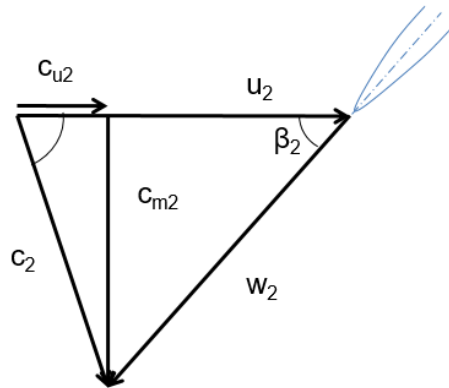


**Figure 2.10:** Velocity triangle for the outlet of a runner. [21]

In order to calculate  $c_{u2}$ , the velocity triangle for the outlet at BEP needs to be used, shown in Figure 2.11. Turbines are designed so that  $c_{u2} = 0$  and  $c_2 = c_{m2}$  at this operating point. The outlet blade angle ( $\beta_2$ ) is constant for all operating points and can therefore be used to calculate  $c_2$  when the turbine is not run at BEP.  $\beta_2$  is calculated using equation (2.27), which is found from Figure 2.11, where  $u_2$  is given in equation (2.28).

$$\beta_2 = \tan^{-1} \left( \frac{c_{m2,BEP}}{u_2} \right) \quad (2.27)$$

$$u_2 = \omega \frac{D_2}{2} \quad (2.28)$$

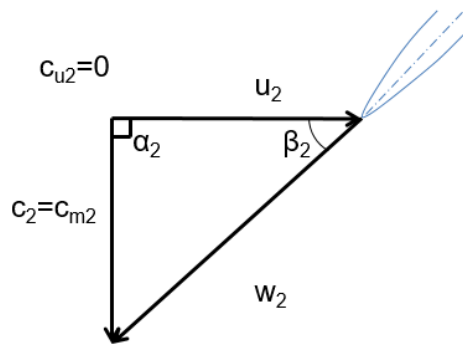


**Figure 2.11:** Velocity triangle for the outlet of a runner at BEP. [21]

When  $\beta_2$  is known, the velocity  $u_2 - c_{u2}$ , seen in Figure 2.10, can be calculated from equation (2.29). As  $u_2$  also is known the expression for  $c_{u2}$  is as seen in equation (2.30).

$$u_2 - c_{u2} = \frac{c_{m2}}{\tan(\beta_2)} \quad (2.29)$$

$$c_{u2} = u_2 - \frac{c_{m2}}{\tan(\beta_2)} \quad (2.30)$$

The values for  $c_{u2}$  and  $c_{m2}$  are then put into equation (2.25) and  $c_2$  is then found.

## Process

A measuring system for measuring and calibrating the axial force was designed and tested for TTL in this Master's thesis. At VKL the axial force is measured using differential pressure transducers, measuring the differential pressure over the hydraulic thrust bearing. This is a complex system and the hydraulic bearings are very sensitive to contaminants. This does not suite the Nepali climate, where the air is full of sand and dust in the dry season. Design of a simpler and cheaper system was therefore attempted. [9] [22]

The idea for the new system is that strain gauges will be placed on the lower part of the bearing block. The strain gauges will measure the strain caused by the axial force when the turbine is running, and the axial force can then be found by comparing the strain values to a calibration curve. When the bearing block for TTL was designed, a spare section was provided in the lower part, designated for the measuring system, seen in Figure 3.1. This section needed further designing in order to be used as a measuring system, and it is this that is the aim of the thesis. It has been re-named as the Axial Load Measuring Device (ALMD) for explanatory purposes.

This chapter explains how the axial force for the runner at TTL has been calculated, how simulations in Ansys Mechanical have been set up and how the experiments were conducted.

### 3.1 Calculation of the axial forces in the turbine

The runner at TTL is a model of the runner at Jhimruk hydropower plant in Nepal. The dimensions of the runner used in the calculations for the axial force can be seen in Figure 2.7 and are based on the technical drawings provided by the TTL staff. Note that the angle  $\phi = 0$  for this runner, meaning that the water enters the runner at an angle of  $0^\circ$ . This implies that  $D_{11} = D_{12}$ , and  $F_1$  is therefore 0 (given in equation (2.8)). From the figure it is also seen that  $D_p = D_{11L}$ , giving that  $F_7$  also is zero (from equation (2.15)).

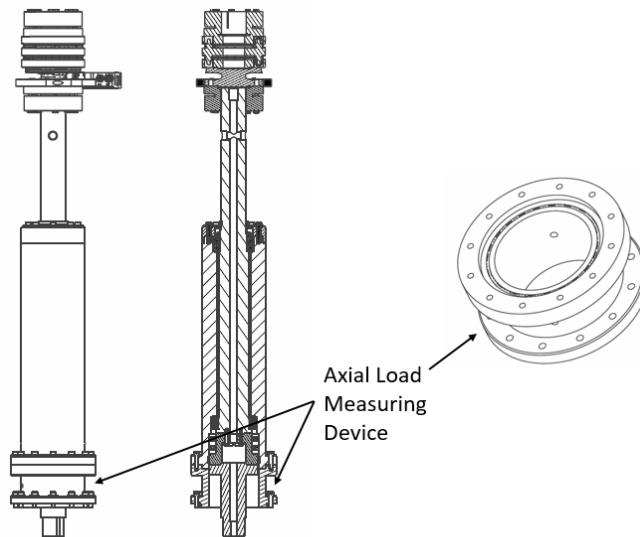


**Figure 3.1:** Full and sectional view of the TTL bearing block, showing the ALMD.

The axial force on the turbine was calculated using the equations given in Section 2.3. Two cases were calculated:

- Case 1: The axial force at BEP
- Case 2: The axial force at maximum flow rate

For both cases, the gauge pressure was used for the calculation. As the gravitational acceleration ( $g$ ) has not yet been measured at TTL,  $g$  was set to  $9.81m/s^2$  in the calculations.

#### Case 1: BEP

The turbine has been designed to have a BEP at  $46m$  net head and  $0.233m^3/s$  flowrate. These values were therefore used to compute the seven axial forces working on the runner. The inlet and outlet pressures ( $h_1$  and  $h_2$ ) were found using equations (2.19) and (2.18) respectively, and were calculated to be  $h_1 = 34.0m$  and  $h_2 = 9.2m$  for this case.

#### Case 2: Max flow rate

The maximum flow rate is achieved when the two pumps run in parallel. A flow rate of  $0.5m^3/s$  is then achieved at a net head of  $75m$ . As with Case 1, the inlet and outlet pressures were calculated using equations (2.19) and (2.18) respectively, giving them a value of  $h_1 = 59.6m$  and  $h_2 = -6.5m$ . The maximum flow rate is the operating point that gives the highest axial force, and is therefore of interest.

**Table 3.1:** Calculated axial forces for the BEP and maximum flow rate cases.

	$F_1[N]$	$F_2[N]$	$F_3[N]$	$F_4[N]$	$F_5[N]$	$F_6[N]$	$F_7[N]$	$F_{total}[N]$
Case 1: BEP	0	-1106	-5198	4804	24490	-22528	0	461
Case 2: Max $Q$	0	-5093	3667	4804	43840	-40250	0	6968

The calculated values of  $F_1 - F_7$ , and the total axial force for both cases can be found in Table 3.1. It can be seen that the highest axial force is just below 7000N (or approximately 700kg), and is the value that has been used in the rest of the thesis as the maximum load. The axial force at BEP is 461N.

## 3.2 Simulations in Ansys Mechanical

The purpose of setting up simulations for the ALMD has been to check the strength of the device in different scenarios. In order to avoid issues with fatigue, the maximum stress in the section should be less than 80% of the yield strength, and the simulations were therefore used to make sure that the maximum stress did not exceed this.

The steel used in the ALMD is *NS-EN 10025 S355 J2+N*. A technical table [23] was used to find the yield strength of the steel, however the exact same material was not found. The yield strength of the *NS-EN 10025 S355 J0* was therefore used instead. The table gave a yield strength of 315MPa – 345MPa. To calculate the maximum stress ( $\sigma_{max}$ ) that should be seen in the ALMD, the lowest value was used, and  $\sigma_{max}$  was calculated to be:

$$\sigma_{max} = 80\% \cdot 315MPa = 252MPa$$

The simulations were set up in Ansys Mechanical 18.1, with the aim to find a suitable wall thickness for the ALMD. The thickness of the wall would be decided based on the maximum stress found in the simulations, which should not exceed 252MPa, and also based on the strain value at the placement of the strain gauges.

First, a mesh independence study was conducted. Small details such as the O-ring and the bevel edges on the flanges were removed as they would not affect the output of the simulations, but would create issues when making the mesh. The ALMD was then split in two main sections, a middle section as seen in Figure 3.2 in blue, and the rest of the ALMD. The middle section was meshed using Element Size on Multiple, which made it possible to set the mesh size to a different one than from the rest of the body, and the Hex Dominant Method was used on the rest of the parts between the two flanges, to force as many hex elements as possible. Quadratic elements were used to avoid issues with shear locking which can occur in linear elements.

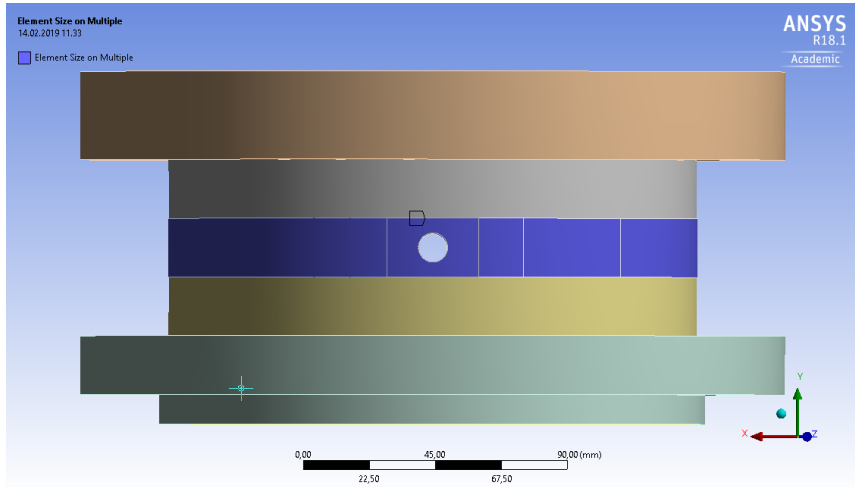


**Figure 3.2:** The middle section of the ALMD in Ansys Mechanical, coloured blue.

The mesh independence study was conducted using Parameter Set. Parameter Set made it possible to run several cases where the mesh size of both the body and the middle section could be changed from case to case. For each case, the maximum stress would be given and mesh convergence would be achieved if the maximum stress did not change much from case to case.

Three cases were run before convergence was achieved. For all the three cases the mesh size on the body was  $4\text{mm}$ , but the mesh size on the middle section was set to  $4\text{mm}$ ,  $3\text{mm}$  and  $2\text{mm}$ . The cases with  $3\text{mm}$  and  $2\text{mm}$  gave close to the same values, and the case with body mesh size of  $4\text{mm}$  and middle section mesh size of  $2\text{mm}$  was therefore used in the simulation. Figure 3.3 shows the mesh.

The model in Ansys Mechanical was set up as accurately to the real model as possible. In the bolt holes in the upper flange, Fixed Support was attached to replicate the bolts holding the ALMD up. In the bolt holes in the lower flange, a force was applied so that the ALMD would be stretched. Several simulations were run, changing the thickness of the wall and varying the force and its direction to check that the ALMD would not yield for any likely scenarios, and the strain was found where the strain gauges would be mounted.



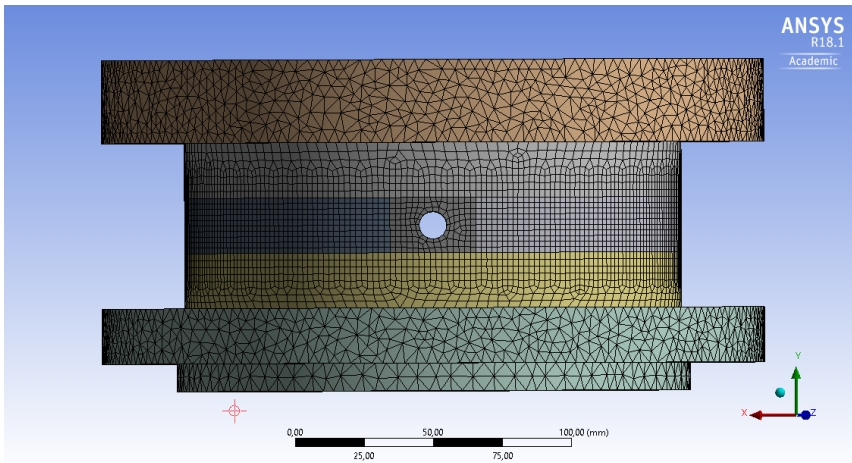


**Figure 3.3:** Mesh used for the ALMD in the simulations.

### 3.3 Experiments

Experiments were conducted at VKL with the purpose of testing the system and checking its behaviour. The experiments were important for two reasons. The first was to see if this was a measuring method that would work, with a predictable behaviour and a satisfactory uncertainty. The second was to find a method for calibrating the system.

To conduct the experiments, the ALMD was manufactured, following the drawings provided by the TTL staff. The machine drawing can be found in Appendix A. The strain gauges needed a flat area to be attached, and four small, flat surfaces were therefore machined on the middle section at an angle of  $90^\circ$  apart.

The experiments were done using a full bridge configuration as described in Section 2.2.1. Two strain gauges were mounted in the axial direction, and two were mounted  $90^\circ$  on the axis as dummy strain gauges, where the pairs were placed on two opposite flat surfaces,  $180^\circ$  apart. Figure 3.4 shows how they were placed. The *S/UCP-120-090* semiconductor strain gauges from Kulite were used for the experiments, and the glue *Z70* from HBM was used to glue them on the section. The strain gauges have a measuring range up to  $3000\mu\text{strain}$  and a gauge factor of 100 [24].

Even though the idea of using a full bridge configuration was to have the strain gauges compensate for temperature, this did not happen. The strain gauges therefore had to be calibrated against temperature. The ALMD, with the mounted strain gauges, was put in a heating cabinet where the temperature would be increased from room temperature to  $50^\circ\text{C}$ . A temperature probe was put on the inside of the ALMD, kept from the air temperature by using insulation and only registering the temperature of the metal. It was left in the heating cabinet overnight to make sure that the temperature stabilized at  $50^\circ\text{C}$ , and then cooled down in the daytime. Each measurement took a day and a night to conduct, and the measurements were repeated 6 times. The measurements would then give a temperature versus  $mV/V$  curve.

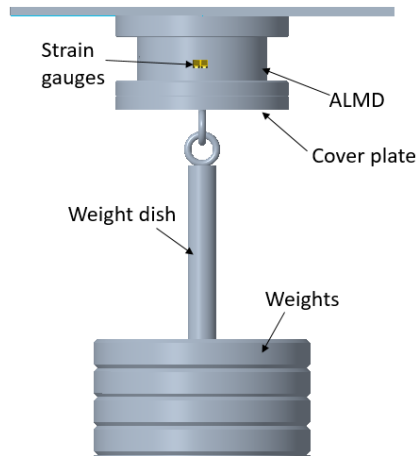


**Figure 3.4:** Test rig for the axial force measurements, also showing the placement of two of the strain gauges. The other two are  $180^\circ$  apart and therefore not visible in the diagram.

From the temperature measurements, a best fit curve was found as a calibration curve for temperature using a fourth order polynomial. Matlab was used to process the data. A mean value from the strain gauges was found for every whole degree, taking the mean of the  $mV/V$  output between  $T - 0.5 \leq T < T + 0.5$  (where  $T$  is the temperature in whole degrees). The room temperature in the laboratory was slightly more than  $23^\circ C$ , so  $24^\circ C$  was the minimum of the curve. To avoid the issues with the fluctuating temperature around  $50^\circ C$  as the heating cabinet was regulated by a thermostat, the curve was cut off at  $48^\circ C$ . The result can be seen in Section 4.2.1.

When a temperature calibration had been made, the load measurements could be obtained. Figure 3.4 shows how the test rig was set up. A flat plate was fastened between two beams at VKL. Underneath the flat plate the ALMD was fastened using 12 bolts. A coverplate with a central hole was fastened to the lower flange of the ALMD, and a ring was fastened in the hole. As the ring was fastened in the middle, the axial force would work equally on all the bolts. A pulley was fastened to the ring to lift the load up and down and a dish was placed at the other end of the pulley to place the weights on. Figure 3.5 shows the experiment.

As the maximum axial force was found to be  $7000N$  (or  $700kg$ ) in Section 3.1, the ALMD was tested for weights between  $0kg$  and  $700kg$ . Thirty-eight calibrated  $5kg$  weights, 5 calibrated  $2kg$  weights and one calibrated  $500kg$  weight were used for the measurements, which meant that the measurements could be conducted stepwise between  $0kg - 200kg$  and  $500kg - 700kg$ . As there were no more calibrated weights that could fill the gap between  $200kg - 500kg$ , measurements could not be made here. The measurements were done following a measurement sequence found in the *DKD-R 6-1 Guideline* [25] shown in Figure 3.6. First three maximum and minimum load measurements were conducted to stress the system, and then two repetitions going stepwise up and down to the maximum and the minimum load were done. Every step was  $20kg$  and the same weights

were taken on and off for the same total weight (i.e. weights number 1, 2, 3 and 4 were put on from  $0\text{kg} - 20\text{kg}$ , and the same weights were taken off from  $20\text{kg} - 0\text{kg}$ ). Every measurement lasted 1 minute, except for the zero load measurement between the two stepped repetitions, which lasted 2 minutes, shown in the sequence. The minimum load was a set zero point. The weight of the pulley, the straps holding the  $500\text{kg}$  load and the weight dish was not allowed to affect the measurements, and the set zero point was therefore the weight of these three items combined.



**Figure 3.5:** Experiment setup for loads below  $200\text{kg}$ .

The data from the strain gauges was sent through a DAQ-unit into a LabVIEW program that would record the measurements for a given amount of time. The strain gauges gave an output in  $mV/V$ , which in equation (2.7) is  $\frac{V_0}{V_{EX}}$ . The data was then saved to an Excel file that was later processed in Matlab.

The tests were done for two wall thicknesses,  $18\text{mm}$  and  $2\text{mm}$ , at the location of the strain gauges. Temperature and load measurements were conducted for the  $18\text{mm}$  case, but only load measurements were conducted for the  $2\text{mm}$  case, due to lack of time. The strain gauges were removed and replaced for the two cases, as they were destroyed during the machining of the  $2\text{mm}$  case. Procedures for doing temperature compensation and calibrating the ALMD can be found in Appendix B and C respectively.

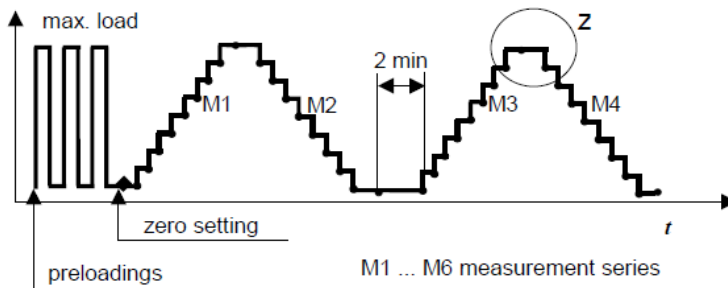


**Figure 3.6:** Measuring sequence recommended in the *DKD-R 6-1 Guideline*. [25]

### 3.3.1 Calibration method

In Selmurzaevs Master's thesis [8] a method for calibrating the axial load was devised without removing the ALMD from the bearing block. This method was considered good enough for TTL and has not been altered. For calibration, the ALMD should be calibrated in both compression and extension, and a system that can calibrate in both upwards and downwards direction is therefore needed.

The principle of Selmurzaevs method is to use a lever beam as seen in Figure 3.7. The beam rotates around a fixed point, so that if a force is applied to point A, point B will experience a force in the opposite direction, making it possible to make the force go upwards. If a force is applied in point C, point B will experience a force in the same direction.

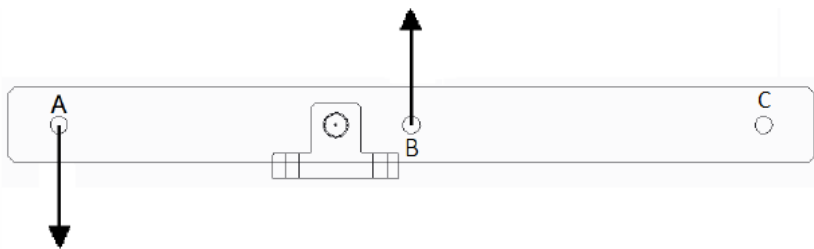


**Figure 3.7:** Lever beam concept recommended by Selmurzaev for calibrating the axial load measuring system. [8]

Point B is connected to the shaft at center point, as can be seen in Figure 3.8. The figure also shows how weights are applied to create a force upwards or downwards, depending on whether the weights are applied in point A or C. The whole system is connected to the turbine housing using four hex bolts, shown in Figure 3.9. Further details on how the system is built up, safety factors and uncertainty analysis can be found in Selmurzaev's Master's thesis [8].



**Figure 3.8:** Axial force calibration system. [8]

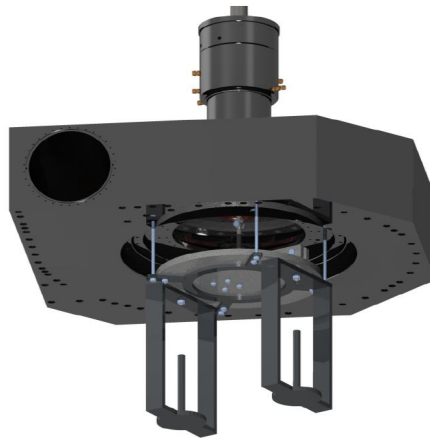


**Figure 3.9:** The axial force calibration system connected to the Francis turbine rig. [8]



# Results and discussion

## 4.1 Numerical analysis

As described in Section 3.2, the aim for the simulations has been to change the wall thickness of the ALMD to a thickness where the strain gauges get a good reading, and at the same time not exceed 80% of the yield strength. Six cases were run, and table 4.1 shows the maximum stress, the strain at the location of the strain gauges and the total deformation for the six cases when a force of  $7000N$  is applied downwards.

Eighty percent of the yield strength was calculated to be  $252MPa$ . It can be seen from Table 4.1 that for even the thinnest wall thickness of  $1mm$ , the maximum stress is far below this value, at only  $42MPa$ . As all the other cases have thicker walls, the maximum stress given for these cases is lower than for case 6.

The strain gauges have an upper limit of  $3000\mu strain$  [24], so this is the maximum strain value the strain gauges should be exposed to. The table again shows that the thinnest wall thickness gives a value far from the upper limit, at a value of  $64\mu strain$ , and that all the other cases give lower values, meaning that case 6 is a good option.

A few simulations were also run to test different scenarios the ALMD could be exposed to, to check the maximum stress in these cases. As there is also a friction torque working on the system, a case where both an axial force of  $7000N$  and a moment of  $20Nm$  was tested. The reason the value of the moment has been set to  $20Nm$  is because the bearings used at TTL are the same as the ones used at VKL. At VKL the friction torque is calibrated between  $0Nm - 20Nm$ , and the friction torque at TTL can therefore be assumed to be the same. Another case with having the axial force work at a slight angle was also tested, in case this would happen in real life. The force was applied at a  $10^\circ$  angle to the original direction, with a value of  $7000N$ . Table 4.2 shows the result for the wall thicknesses of  $1mm$  and  $2mm$ . It can be seen that the maximum stress does not change much for the  $1mm$  case when the moment is applied, but for the  $2mm$  case it increases somewhat. The maximum stress increases quite a bit more for both wall thicknesses when the force is applied at an angle, but is still far below the upper limit of  $252MPa$ . Both these analyses conclude that a wall thickness of  $1mm$  can be used.

**Table 4.1:** Results from the simulations in Ansys Mechanical when a force of 7000N is applied downwards.

Case	Wall thickness (mm)	Max stress (Mpa)	Strain at placement of strain gauges (mm/mm)	Max total deformation (mm)
1	18	6.72	$8.8481 \times 10^{-6}$	0.0028172
2	10	8.55	$4.7097 \times 10^{-6}$	0.003253
3	5	12.115	$2.7993 \times 10^{-6}$	0.0055212
4	3	18.822	$1.0826 \times 10^{-5}$	0.007913
5	2	24.478	$2.5423 \times 10^{-5}$	0.0099936
6	1	42.036	$6.4025 \times 10^{-5}$	0.013768

**Table 4.2:** Comparing the maximum stresses in different scenarios for 1mm and 2mm wall thickness.

Wall thickness (mm)	Strain at 7000N (mm/mm)	Max stress at 7000N (MPa)	Max stress with the force at a 10° angle (MPa)	Max stress at 7000N and 20Nm (MPa)
2	$2.5423 \times 10^{-5}$	24.478	33.785	28.702
1	$6.4025 \times 10^{-5}$	42.036	49.622	42.035

Figures 4.1, 4.2 and 4.3 show the distribution of the stress, strain and total deformation in the ALMD for a 2mm wall thickness. It can be seen that the area around the lower flange is the part of the ALMD that gets the greatest values, both for stress, strain and total deformation. The area where the strain gauges are placed is somewhat exposed, but not the most exposed area.



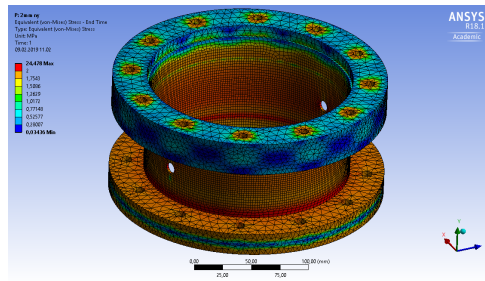


Figure 4.1: Distribution of stress for the 2mm wall thickness.

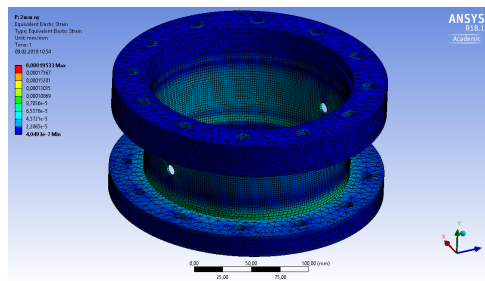


Figure 4.2: Distribution of strain for the 2mm wall thickness.

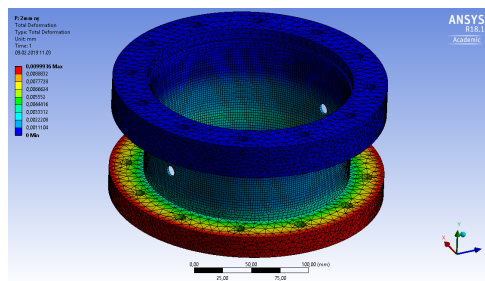


Figure 4.3: Distribution of deformation for the 2mm wall thickness.

## 4.2 Experiments

As described in Section 3.3, experiments were conducted for two wall thicknesses,  $18mm$  and  $2mm$ . The system proved dependent on temperature, and a temperature compensation therefore had to be done. However, there was only time to do it for the  $18mm$  wall thickness.

In the following sections, the  $18mm$  case has been referred to as Experiment 1, and the  $2mm$  case as Experiment 2. Even though the numerical analysis showed that a wall thickness of  $1mm$  was viable, the ALMD was tested at  $2mm$  after discussions with technical and academic staff at VKL.

This section first describes the temperature compensation for Experiment 1 and then the load measurements for both experiments. Subsection 4.2.4 compares the results from the two experiments, and Subsection 4.3 compares the experiments to the simulations in Ansys.

### 4.2.1 Experiment 1, Temperature Compensation

The temperature compensation was conducted as described in Section 3.3. Six measurements were made, giving the  $mV/V$  output from the strain gauges for the whole temperature range tested for. The first measurement gave a very different curve, likely due to the glue setting, and was deleted in the further analysis. The other measurements showed good repeatability.

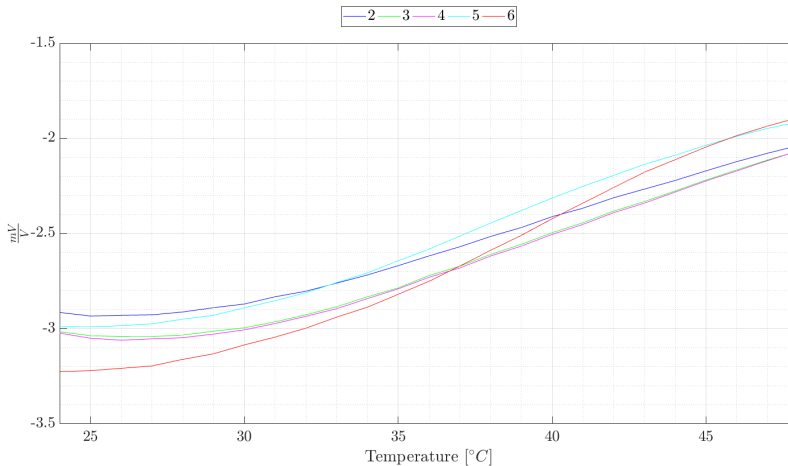


**Figure 4.4:** Temperature curves for the  $18mm$  wall thickness.

Figure 4.4 shows the result for measurements 2-6. It can be seen that the output from the strain gauges varies a lot with temperature, demonstrating the need for temperature compensation. For measurement 6 for example, the  $mV/V$  output varied between  $-3.23mV/V$  and  $-1.89mV/V$ , giving a difference of  $1.34mV/V$ .

To make a temperature compensation curve, a best fit curve was found for the five temperature measurements, as described in Section 3.3. The curve is shown in Figure 4.5 and is a fourth order polynomial, given by the equation (4.1).

$$y_{temp} = 7.17 \times 10^{-8}T^4 - 1.20 \times 10^{-4}T^3 + 0.01T^2 - 0.46T + 1.92 \quad (4.1)$$

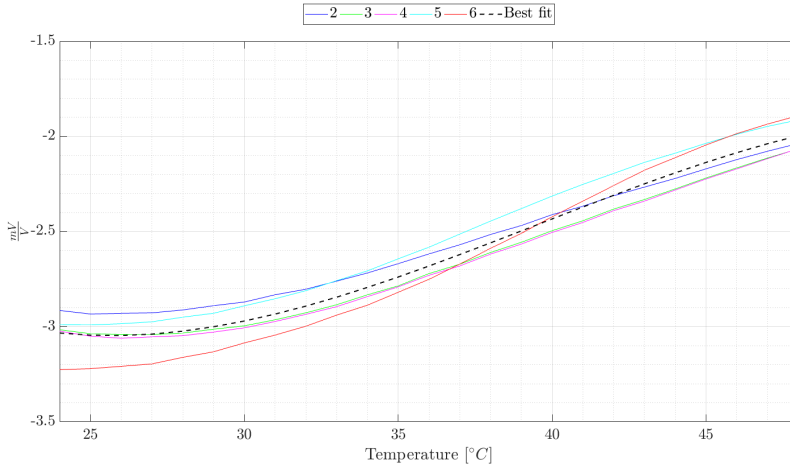


**Figure 4.5:** Best fit line for the temperature curves for the 18mm wall thickness.

To compensate the measurements for temperature, the best fit curve needed to be subtracted from the measured data. Figure 4.6 shows the result when this has been done. The measurements are now close to the  $0mV/V$  line, fluctuating between  $-0.2mV/V$  –  $2mV/V$ . The curves stay relatively flat for the whole temperature range, which is the desired response.

The temperature curves were plotted between  $24^{\circ}C$  –  $48^{\circ}C$  as the room temperature in the laboratory was above  $23^{\circ}C$ . When the load measurement was conducted, the room temperature was between  $20.8^{\circ}C$  –  $21.15^{\circ}C$ , meaning that the temperature compensation curve could not be used for these data points. The curve was however extrapolated from the values between  $24^{\circ}C$  –  $28^{\circ}C$  to  $20.8^{\circ}C$  and  $21.15^{\circ}C$ . The difference in output at these temperatures was found to be  $0.0012mV/V$ , and was considered so small that it would not overshadow the uncertainty in the load measurements. Temperature compensation was therefore not used for either Experiment 1 or Experiment 2.

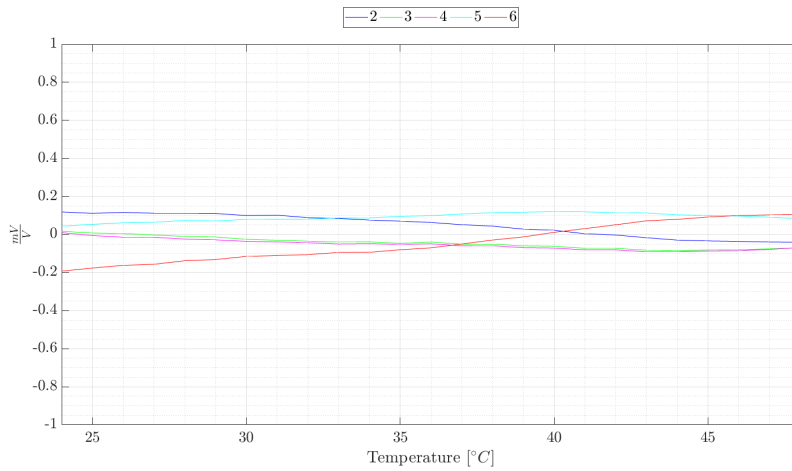


**Figure 4.6:** Temperature curves for the 18mm wall thickness after temperature correction has been done.

### 4.2.2 Experiment 1, Load Measurement

The result from Experiment 1 can be seen in Figure 4.7. The first three peaks are where the system is being tested under maximum strain, and are not a part of the actual calibration. The three peaks show that the maximum and minimum loads do not repeat themselves well, as both are increasing for the three measurements.

The two stepped peaks are the two repetitions where loads have been added  $20kg$  at a time, and the big leap is where the jump from  $200kg$  to  $500kg$  happens. It looks like the repetitions replicate well, although Repetition 2 looks to lie slightly below Repetition 1. In the measurements between  $200kg - 0kg$  for Repetition 2, something went wrong, and for this reason, M4 has been deleted in the calculations.

Above  $500kg$  hysteresis has a major effect, and results for increasing loads are not identical to the results for decreasing loads. The hysteresis gets increasingly pronounced when off-loading from  $700kg$  to  $500kg$ . Below  $200kg$  the hysteresis seems to be small, as the values for the on-loading and off-loading look to be approximately the same.

The zero load measurements also seem to repeat themselves well, indicating that the zero load deviation will be small.

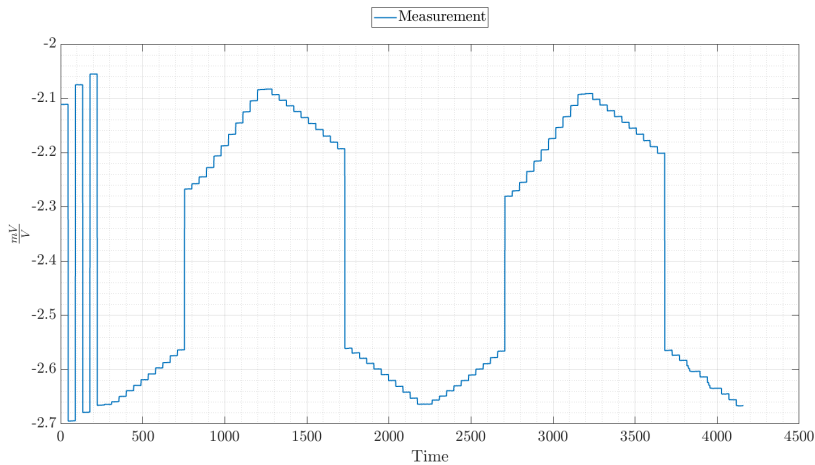


**Figure 4.7:** Axial load measurement for the 18mm wall thickness.

To more easily compare the two repetitions, they have been superimposed in Figure 4.8. For the on-loading below  $200\text{kg}$  the two repetitions seem to follow each other almost perfectly, but for the off-loading in the same load range Repetition 1 lies slightly above Repetition 2. However it is difficult to say anything exact about Repetition 2 here as some measuring points are invalid. Above  $500\text{kg}$  the two repetitions seem to replicate well with each step being approximately the same, however Repetition 1 lies above Repetition 2.

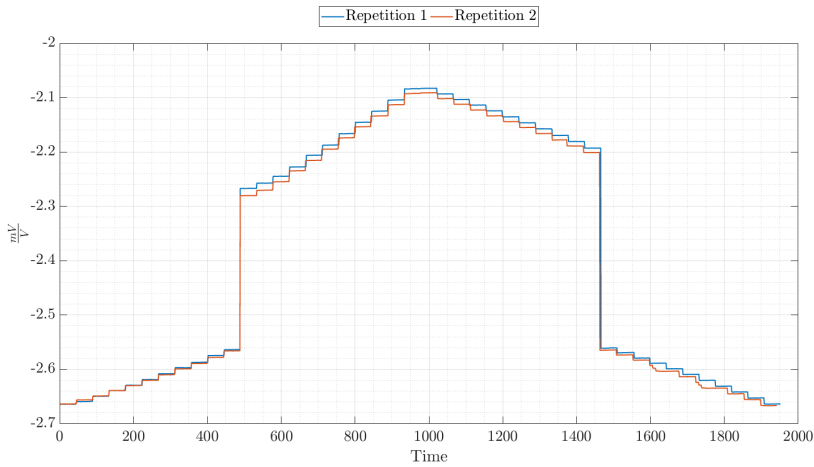


**Figure 4.8:** The two repetitions superimposed for the 18mm wall thickness.

Figure 4.9 shows the value of every measurement at the different loads, where the red dots represent the on-loading and the blue dots the off-loading. The gray area is the area where measurements could be made. The figure makes it obvious that the hysteresis is large above  $500\text{kg}$ , with the blue dots lying far above the red ones. The hysteresis narrows as the loads get added above  $500\text{kg}$ . It can also be seen that the values for the on-loading are very similar below  $200\text{kg}$ , but are slightly wider above  $500\text{kg}$ , as was also seen in Figure 4.7 with Repetition 1 lying slightly above Repetition 2.

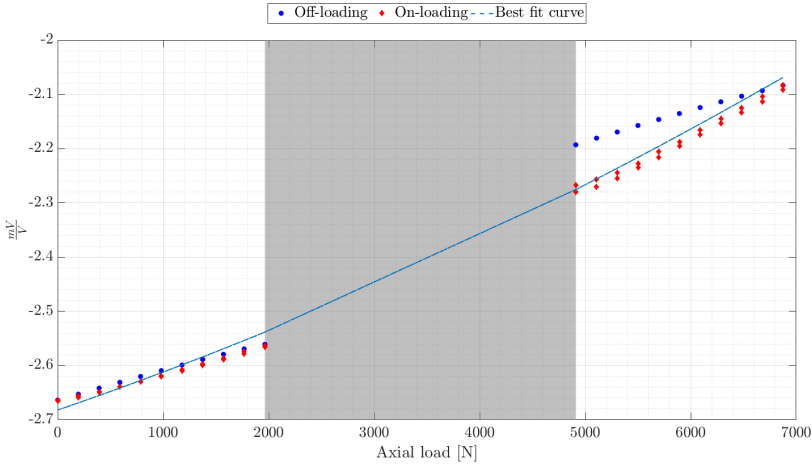


**Figure 4.9:** Measuring points for the on-loading and off-loading for the 18mm wall thickness. The best fit curve is plotted between the data points.

To calibrate the system, a calibration curve was made as a best fit curve between the data points. As strain gauges in a Wheatstone bridge have a linearity error, a second order polynomial should be used [26]. This was however tested. Both a first and a second order polynomial were tested as possible best fit curves. Figures 4.10 and 4.11 show the deviation between the modelled load and the actual load for the first order and second order case, respectively. It is desirable to have the deviation as small as possible, where a deviation of zero means that the model fits the measurements perfectly. As seen in the figures, the curves for the deviation have a similar shape. The first order polynomial starts with a deviation around  $400N$  for a  $0kg$  load, where the second order polynomial has a somewhat smaller deviation of  $260N$ . When increasing the load from  $0kg - 200kg$ , the deviation gets smaller, but once it has reached 0, it starts increasing again, this time to a negative value. At  $200kg$  the deviation is again very large. Above  $500kg$  the deviation is a lot less pronounced for the first order than the second order, where the deviation for the first order polynomial in fact approaches 0 as more loads are added.

There is however no obvious model that fits the measurements best from among the tested best fit curves. Because of the linearity error in the Wheatstone bridge, the second order polynomial was chosen, and can be seen in Figure 4.9. The curve looks to be almost linear, which explains why the two deviation curves looked similar. It should however be noted that when the deviation is as large as it is for this system, the error when doing axial force measurements will be great.

The curve is given by equation (4.2).

$$y_{Exp.1} = 3.27 \times 10^{-9}x^2 + 6.67 \times 10^{-5}x - 2.68 \quad (4.2)$$

From Figure 4.9 it can be seen that the curve does not fit the data points very well and there is therefore a great deal of uncertainty in the system.

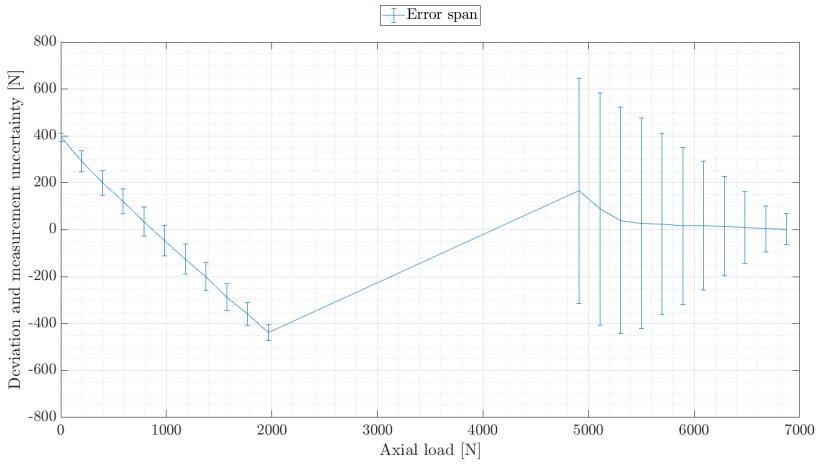


**Figure 4.10:** Deviation between modelled and actual load for the 18mm wall thickness using a first order polynomial.

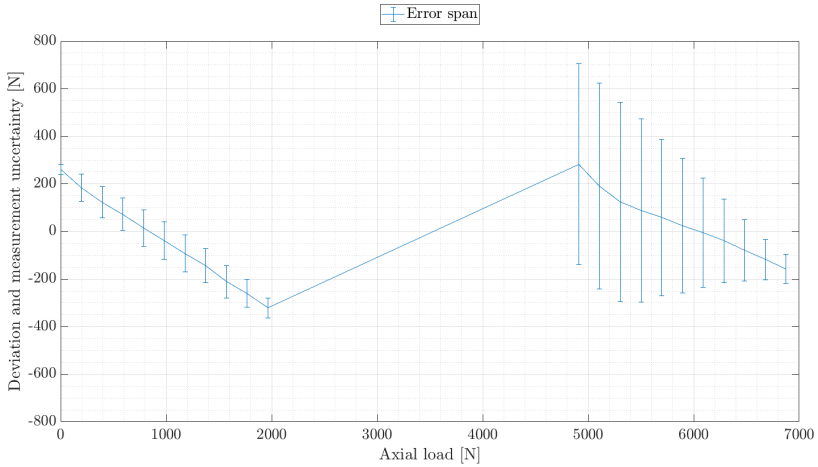


**Figure 4.11:** Deviation between modelled and actual load for the 18mm wall thickness using a second order polynomial.



### Uncertainty analysis

The uncertainty analysis was conducted based on the *DKD-R 6-1 Guideline* [25] for one full repetition, but three measurement series. The mean value ( $M_{iw}$ ), hysteresis ( $h$ ) and repeatability ( $b'$ ) were found using equations (4.3), (4.4), (4.5), respectively.

$$M_{iw} = \frac{\sum M_i}{3} \quad (4.3)$$

$$h_{mean,j} = |(x_{2,j} - x_{1,0}) - (x_{1,j} - x_{1,0})| \quad (4.4)$$

$$b'_{mean,j} = |(x_{3,j} - x_{3,0}) - (x_{1,j} - x_{1,0})| \quad (4.5)$$

Here,  $i$  is the number of the measurement series in question, i.e. M1, M2 or M3, and  $j$  is the measurement number. The hysteresis and repeatability are calculated from the zero load measurement.

The zero deviation ( $f_0$ ) was also found using equation (4.6).

$$f_0 = |x_{2,0} - x_{1,0}| \quad (4.6)$$

As there were only three measurements for each load, the uniform distribution was used to find the uncertainty.  $u(x_i) = \frac{2a}{2\sqrt{3}}$  was therefore used to calculate the uncertainty. Table 4.3 in Section 4.2.3 shows the calculation of one value. The total uncertainty ( $U_{total}$ ) was calculated using equation (4.7), where  $k = 1.96$  for a 95% confidence interval.

$$U_{total} = k\sqrt{u_{f_0}^2 + u_{b'}^2 + u_h^2} \quad (4.7)$$

The total error for the system can be seen in Figures 4.12 and 4.13, where Figure 4.12 shows the absolute error for each load, and Figure 4.13 shows the percentage error for the load. It should be noticed that the error range bars are superimposed on the modelled values, which, as discussed earlier, deviate quite a lot from the actual load in Figure 4.11. From Figure 4.13 it can be seen that the greatest percentage error happens at a load of 20kg, where the error is 15%. From the 20kg load the error diminishes when the load increases towards 200kg, and lies around 2% – 3% for the 200kg load. After the jump to 500kg, the error increases again, reaching approximately 8% maximum, then decreasing again as more loads are added, ending up around 1% for the 700kg load.

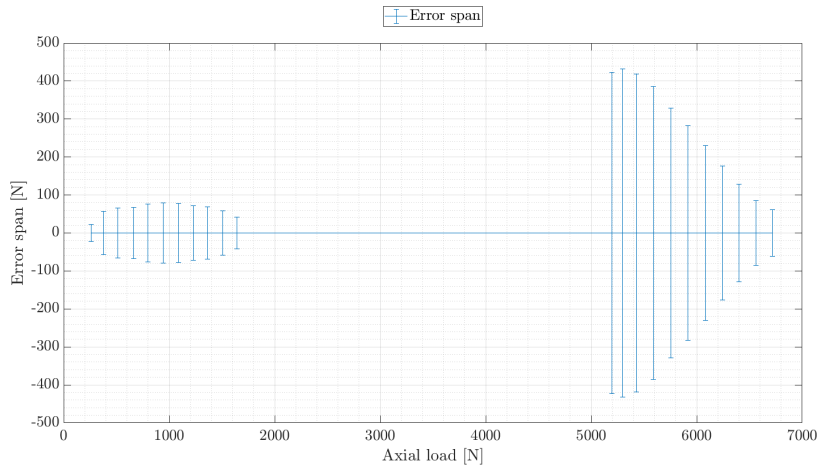


**Figure 4.12:** The absolute range of error for the modelled loads at a wall thickness of 18mm.

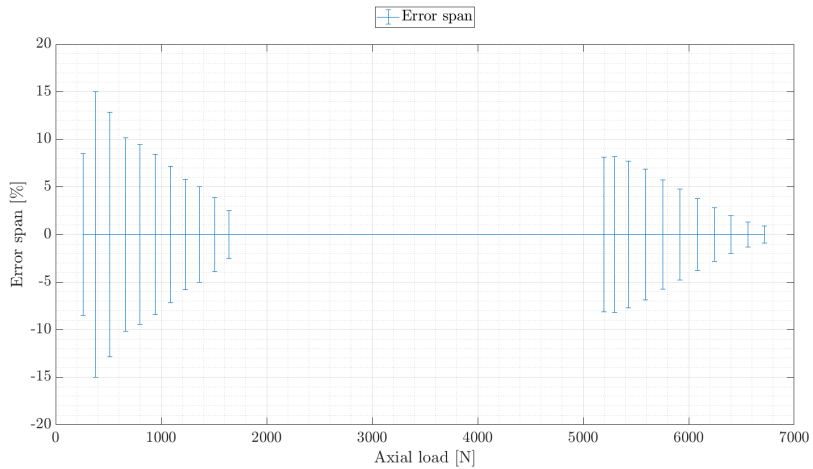


**Figure 4.13:** The percentage range of error for the modelled loads at a wall thickness of 18mm.

Figure 4.14 shows the contribution from the hysteresis, repeatability and zero deviation to the total error. It can be seen that the error from the zero deviation is small, meaning that the different zero loads gave close to the same value, as was also seen in Figure 4.7. The biggest contributor to the error is the hysteresis. Below  $200\text{kg}$  it stays quite constant for a majority of the loads, but decreases slightly for the highest loads. At  $500\text{kg}$  the hysteresis is large, as was also predicted from Figure 4.8. However, it decreases as the loads are further increased. This is probably the reason why the total error increases after the jump to  $500\text{kg}$  as seen in Figure 4.13, but decreases as the load is further increased. The error caused by the repeatability starts off being very small but increases somewhat as more loads are added.

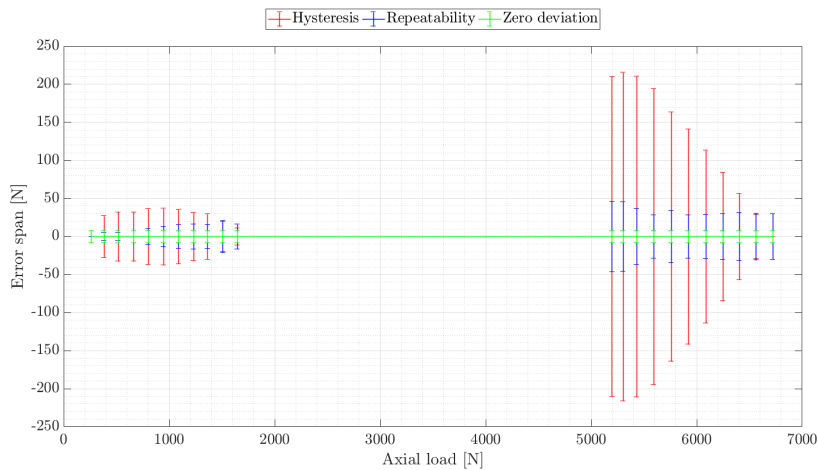


**Figure 4.14:** The contribution from the hysteresis, repeatability and zero deviation to the total error for the 18mm wall thickness.

### 4.2.3 Experiment 2, Load Measurement

The result from Experiment 2 can be seen in Figure 4.15. The first three peaks are the maximum load measurements conducted prior to the two stepped repetitions. It can be seen that they do not repeat the exact same value for the same maximum load, but they are all between  $11.95 - 12.000 \text{ mV/V}$ . The zero load measurements are also non-identical for the three repetitions.

The two stepped repetitions seem to repeat themselves well. The big discontinuity in the middle is where the jump from  $200\text{kg} - 500\text{kg}$  or  $500\text{kg} - 200\text{kg}$  happens. For the loads above  $500\text{kg}$ , the hysteresis appears to be large, although it decreases when the load increases. Up to  $200\text{kg}$  the hysteresis is smaller, yet still visible. The value for the zero load measurements seems to increase for every repetition, and might be what causes the apparent hysteresis in this lower part of the graph. The  $500\text{kg}$  load measurement both before and after the discontinuity seems to be close to the same value for the two on-load and two off-load measurements, implying that it might be independent of the increase in zero load measurement.

An invalid measurement was obtained in the second repetition after the jump between  $200\text{kg} - 500\text{kg}$  which has been deleted in the rest of the analysis.

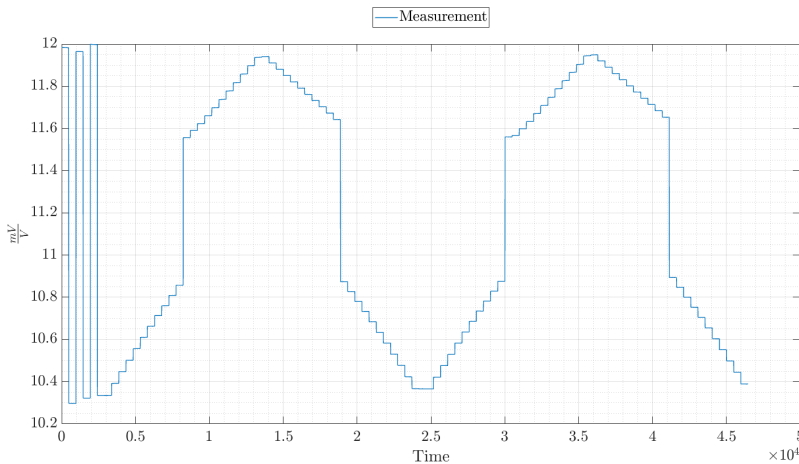


**Figure 4.15:** Axial load measurement for the 2mm wall thickness.

To more easily see how well the two repetitions repeat themselves, they have been plotted on top of each other in Figure 4.16. In the figure it looks as if the repetitions replicate well, with each step between each measurement being very similar. However, Repetition 2 has a higher zero load reading that makes it lie slightly above Repetition 1 for the measurements below  $200\text{kg}$ . Above  $500\text{kg}$  this difference is smaller.

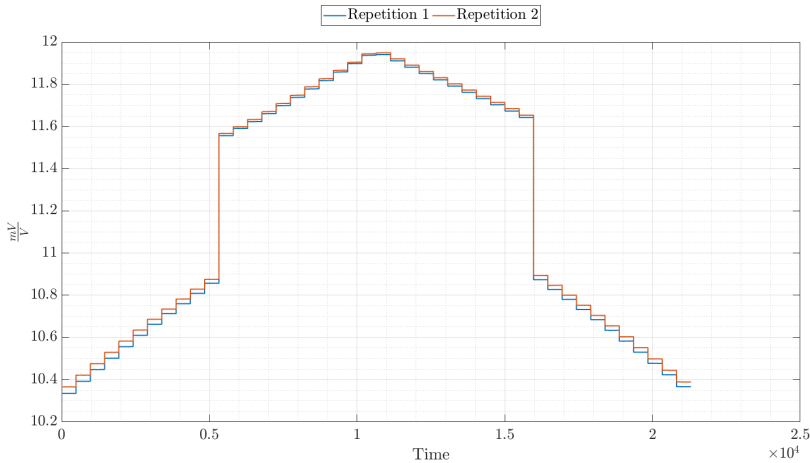


**Figure 4.16:** The two repetitions superimposed for the 2mm wall thickness.

Figure 4.17 shows the value for every measurement at a certain axial force, where the red dots represent the on-loading (M1 and M3) and the blue dots represent the off-loading (M2 and M4). The grey area in the middle is the jump between  $200kg - 500kg$  where no measurements could be taken. From the figure it is obvious that the difference between the on-loading and off-loading above  $500kg$  is large, meaning that the hysteresis is also large. It can also be seen that the difference between M1 and M3, and M2 and M4 is greater below  $200kg$  than above  $500kg$ , as was also seen in Figure 4.16.

To create a calibration curve, a best fit line was found for the measurements. Both a first order and a second order polynomial were tested as best fit curves to see which one was the best option, as for Experiment 1. Figures 4.18 and 4.19 show the deviation between the modelled load and the actual load for a first and second order polynomial respectively. A smaller deviation means that the model fits the measurements better and is therefore desirable. Comparing the figures it is obvious that the second order polynomial is the better option. The first order polynomial gives higher deviations in general, and especially at the  $0kg$  and  $500kg$  loads, making it a less accurate model.

In Figure 4.17 the best fit curve is plotted between the data points, and is given by equation (4.8).

$$y_{Exp.2} = -8.81 \times 10^{-9}x^2 + 2.92 \times 10^{-4}x + 10.35 \quad (4.8)$$

From the figure it is seen that there is some deviation between the best fit line and the actual measurements. This implies uncertainty in the model and an uncertainty analysis has therefore been conducted.

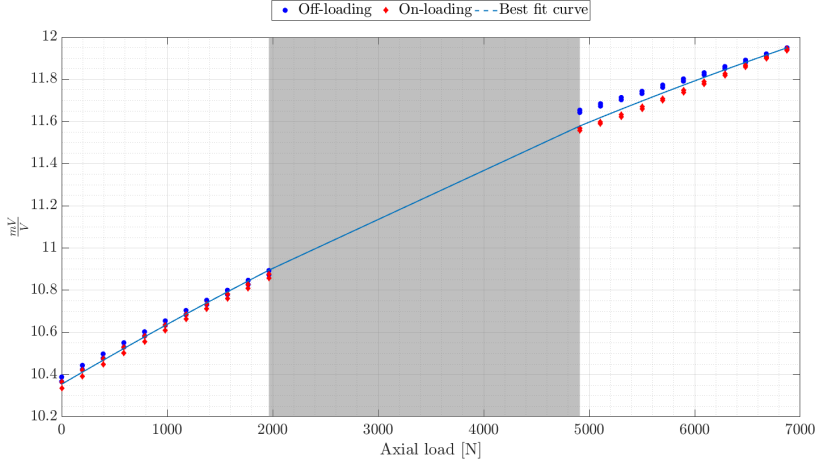


**Figure 4.17:** Measuring points for the on-loading and off-loading for the 2mm wall thickness. The best fit curve is plotted between the data points.

### Uncertainty analysis

As with Experiment 1, the uncertainty analysis has been conducted based on the *DKD-R 6-1 Guideline* [25], but this time for four measuring points. The mean value, hysteresis and repeatability are found for every measuring point, using equations (4.9), (4.10) and (4.11) respectively.

$$M_{iw} = \frac{\sum M_i}{4} \quad (4.9)$$

$$h_{mean,j} = \frac{1}{n} [ |(x_{2,j} - x_{1,0}) - (x_{1,j} - x_{1,0})| + |(x_{4,j} - x_{3,0}) - (x_{3,j} - x_{3,0})| ] \quad (4.10)$$

$$b'_{mean,j} = \max(b'_{up,j}, b'_{down,j}) \quad (4.11)$$

where

$$b'_{up,j} = |(x_{3,j} - x_{3,0}) - (x_{1,j} - x_{1,0})| \quad (4.12)$$

$$b'_{down,j} = |(x_{4,j} - x_{4,0}) - (x_{2,j} - x_{2,0})| \quad (4.13)$$

The zero deviation ( $f_0$ ) was also found using equation (4.14).

$$f_0 = \max(|x_{2,0} - x_{1,0}|, |x_{4,0} - x_{3,0}|) \quad (4.14)$$

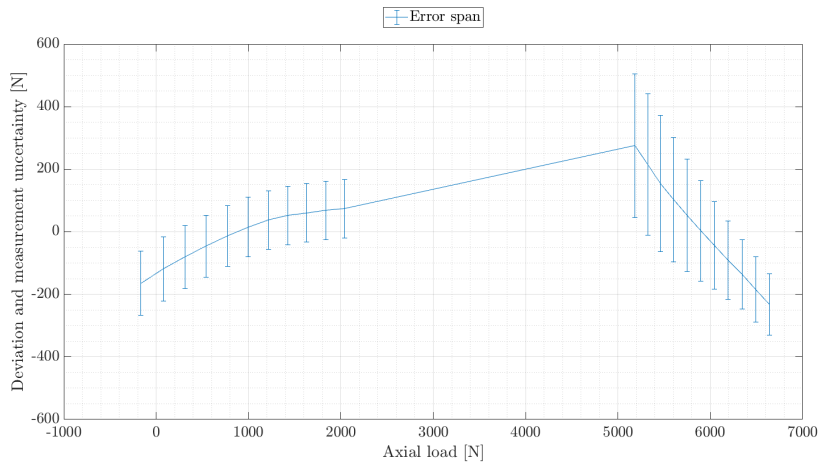


**Figure 4.18:** Deviation between modelled and actual load for the 2mm wall thickness using a first order polynomial.

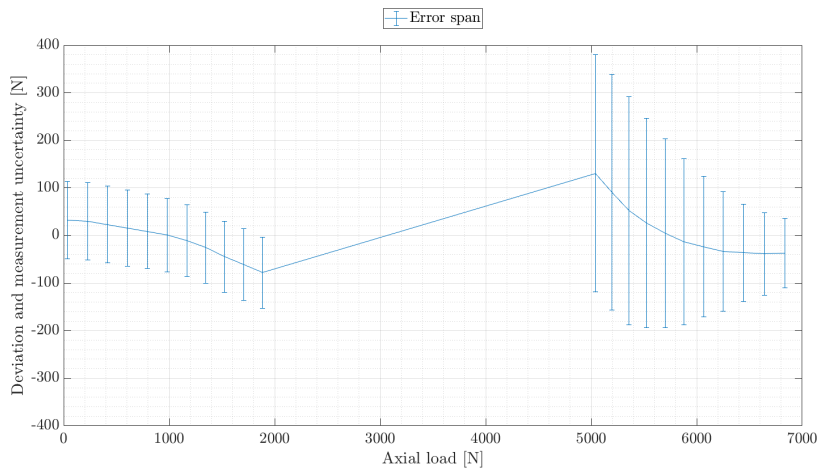


**Figure 4.19:** Deviation between modelled and actual load for the 2mm wall thickness using a second order polynomial.

**Table 4.3:** Calculation of the errors in load step  $F = 196.44N$  at a wall thickness of 2mm.

Quantity	Width of distribution	Divisor	Uncertainty	Percentage uncertainty	Variance
$X$	$2a$		$u(x_i)$	$u(x_i)$	$u^2$
$F_{f_0}$	$109.20N$	$\sqrt{3}$	$31.52N$	16.05%	993.73
$F_{b'}$	$4.69N$	$\sqrt{3}$	$1.35N$	0.69%	1.83
$F_h$	$93.28N$	$\sqrt{3}$	$26.93N$	13.71%	725.12
$U_{total}$			80.30N		

The uniform distribution was also applied to Experiment 2, as there were only four measurement points for every load.  $u(x_i) = \frac{2a}{2\sqrt{3}}$  was used to calculate the uncertainty and equation (4.7) was used to find the total uncertainty, where  $k = 1.96$  for a 95% confidence interval. Table 4.3 shows the calculations of the errors for a force of  $F = 196.44N$ , and the same calculations have been performed for all the other measurement points. The table shows that the zero deviation contributes the largest uncertainty, with the hysteresis close behind for this force value. The uncertainty from the repeatability is small at less than 1%.

The total error for all the measurement points can be seen in Figure 4.20, and the error in percent of the load can be seen in Figure 4.21. In Figure 4.21 it is seen that the error is very large at the smaller loads, with the error being 36% for a 20kg load and almost 20% for a 40kg load, but decreases as the load increases. When the load jumps from 200kg to 500kg the error increases slightly before decreasing again, ending up below 2% for a 700kg load.



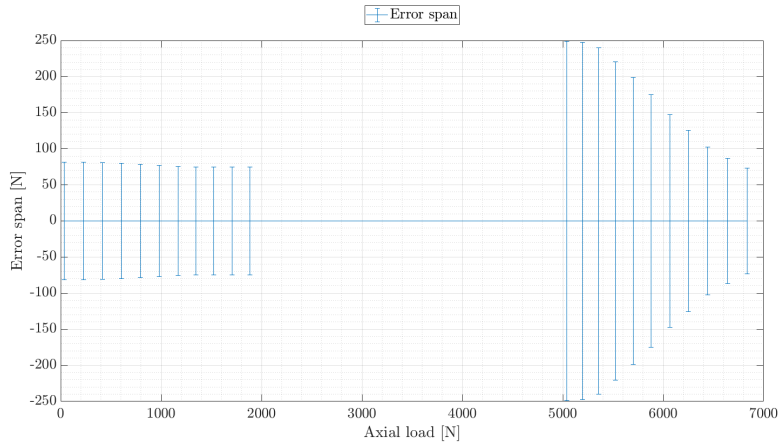


**Figure 4.20:** The absolute range of error for the modelled loads at a wall thickness of 2mm.

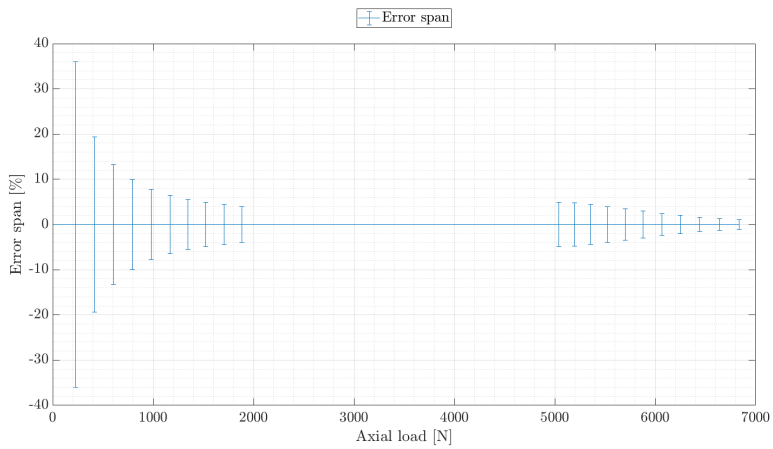


**Figure 4.21:** The percentage range of error for the modelled loads at a wall thickness of 2mm.

Figure 4.22 shows the contribution of the hysteresis, zero deviation and repeatability for the total error at every measurement point. From the figure it is seen that the repeatability is the error that contributes the least to the total error, as was also assumed from Figures 4.15 and 4.16. Below  $200kg$  the error from the zero deviation is the biggest contributor to the total error with the hysteresis as a good second. After the jump to  $500kg$  the hysteresis becomes large and is the biggest contributor. Comparing this finding with Figure 4.21, this might be the main reason for the increasing error between  $200kg$  and  $500kg$ .

A trend can be seen for the hysteresis, where it for  $0kg - 200kg$  decreases when more loads are added, and the same happens for  $500kg - 700kg$ . The reason why the hysteresis suddenly gets so large at  $500kg$  might therefore be because of the jump between  $200kg - 500kg$ . If loads could be applied more gradually in this gap, the hysteresis might behave differently and follow the trend of decreasing for higher loads.

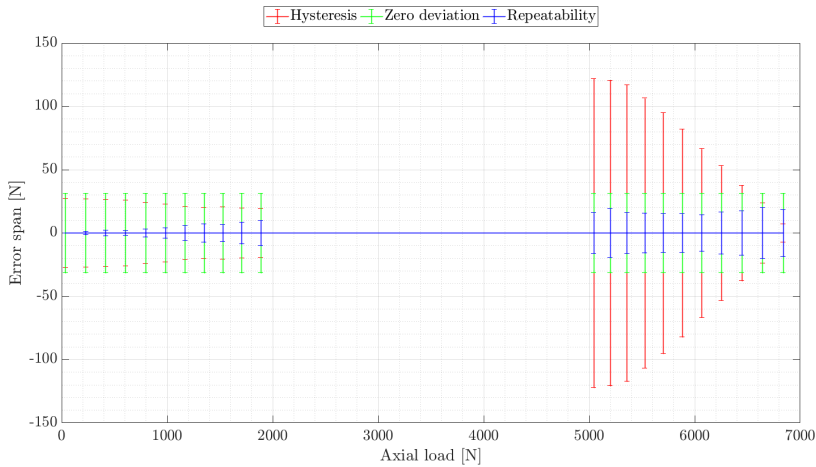


**Figure 4.22:** The contribution from the hysteresis, repeatability and zero deviation to the total error for the 2mm wall thickness.

#### 4.2.4 Comparing the experiments

In order to see if changing the wall thickness has given a better result, the two experiments are compared.

##### **Zero load deviation**

The zero load deviation was small for Experiment 1, with the zero load measurement not changing much at all. This was not the case for Experiment 2, where the zero load measurement changed a lot for all the three measurements and was a big contributor to the total error, especially below  $200\text{kg}$ . It should however be pointed out that the zero load deviation for Experiment 1 was based on only two values, whereas it was based on three for Experiment 2, making Experiment 2 more reliable in theory. From Figure 4.7 however, it looks like the third zero load measurement for Experiment 1 (that was later deleted), also is close to the other zero load measurements, and that the deviation would have stayed small if all three measurements had been used.

It is hard to say why the zero load deviation was larger for Experiment 2 than for Experiment 1. One theory could be that the Experiment 2 system was much more sensitive as the wall thickness was much thinner. To check this it could be a good idea to repeat the experiment and see if it happens again. It is however relatively normal that the zero load changes during an experiment, and it should therefore be compensated for during the measurements.

##### **Repeatability**

The repeatability behaves similarly for both experiments. For both experiments the steps for the same load looked to be very similar for the two repetitions, but in both cases one of the repetitions would lie slightly above the other. For Experiment 2 this might have been caused by the zero load deviation. Below  $200\text{kg}$  this error would not be corrected, and the repeatability would suffer as a consequence. For Experiment 1 there does not seem to be any good explanation, as it happened for the loads above  $500\text{kg}$ . One reason could however be that something happened in the jump between  $200\text{kg} - 500\text{kg}$  that could disrupt the system.

When comparing Figures 4.14 and 4.22 it is seen that the error from the repeatability is higher for Experiment 1 than for Experiment 2, meaning that a thinner wall has made the measurements more accurate. The fact that both experiments repeat themselves well is good for measuring purposes. It means that the same measured value will be caused by approximately the same force every time.

### Hysteresis

The hysteresis has in both cases been the biggest contributor to the total error, especially for the values above  $500\text{kg}$ . For Experiment 2 it looked like the hysteresis decreased for increasing loads between  $0\text{kg} - 200\text{kg}$ , but after the jump to  $500\text{kg}$  it again increased before decreasing for higher loads. A similar trend was seen for Experiment 1, even though the hysteresis was quite constant below  $200\text{kg}$ . If experiments could have been made in the  $200\text{kg} - 500\text{kg}$  gap, the trend of the hysteresis decreasing for higher loads might have been continued.

Comparing the values of the hysteresis for the two experiments shows that below  $200\text{kg}$  the hysteresis looks to be approximately the same value for both experiments, but above  $500\text{kg}$  the hysteresis is approximately twice as large for Experiment 1 as for Experiment 2. This means that making the wall thinner has helped make the hysteresis smaller.

It cannot be said for certain why the hysteresis ends up being so large, but tests should be done to try to make it smaller. One theory is that the glue behaves differently in compression versus extension, and that this becomes very obvious at high loads. As the strain gauges should be able to measure up to  $3000\mu\text{strain}$ , they should not be the cause of the hysteresis.

### Total error

Comparing Figures 4.13 and 4.21 shows that generally the total error is smaller for Experiment 1. It is seen that the total error starts off being very large for Experiment 2, with an error of approximately 36% at a load of  $20\text{kg}$ . The error drops rapidly to about 4% for a  $200\text{kg}$  load, and increases slightly after the gap between  $200\text{kg} - 500\text{kg}$ , before decreasing towards  $700\text{kg}$ . For Experiment 1 a similar trend can be seen, but the total error is maximally 15%, also at  $20\text{kg}$ . After the jump from  $200\text{kg}$  to  $500\text{kg}$  the total error is somewhat bigger than for Experiment 2, but once the maximum load is reached, the total error is again smaller for Experiment 1.

This result is surprising as it would be expected that the error and accuracy would be better for a thinner wall thickness, as a greater output would be given by the strain gauges. It is however likely that the large deviation in zero load measurements for Experiment 2 is what has made the total error of the system generally larger for Experiment 2. After the jump to  $500\text{kg}$  the error for Experiment 1 is likely to be larger because the hysteresis here is so much greater for Experiment 1 than for Experiment 2.

At the best efficiency point for the runner at TTL, the axial force is calculated to be  $461\text{N}$ , which is equivalent to a load just below  $50\text{kg}$ . At this load, the error in both experiments is large, meaning that using this system around the BEP will give a high uncertainty in the results. This system can however be used if the axial bearing is designed for such a large uncertainty.

### Deviation between modelled and actual load

The deviation between the modelled loads and the actual load, is what tells how well the best fit curve fits. Figure 4.23 shows the deviation between the modelled and actual loads for both experiments. It can easily be seen that Experiment 2 fits a lot better than Experiment 1, which could also be seen when comparing Figures 4.11 and 4.19 and also when plotting the best fit curve with the data points in Figures 4.9 and 4.17. The best fit curve is the calibration curve, based on the measurements obtained from the known weights. If the calibration curve is not accurate it will not predict the correct force for any given  $mV/V$  reading. This was made apparent for Experiment 1, where the calibration curve indicated that a  $0kg$  load represented a force of  $260N$ , which should obviously have been  $0N$ .

The fact that the deviation is so large for Experiment 1 makes it unsuitable as a measuring device. For Experiment 2 this deviation was a lot smaller, implying that a thinner wall thickness, and thereby a larger strain gauge output, would give a better measuring system.

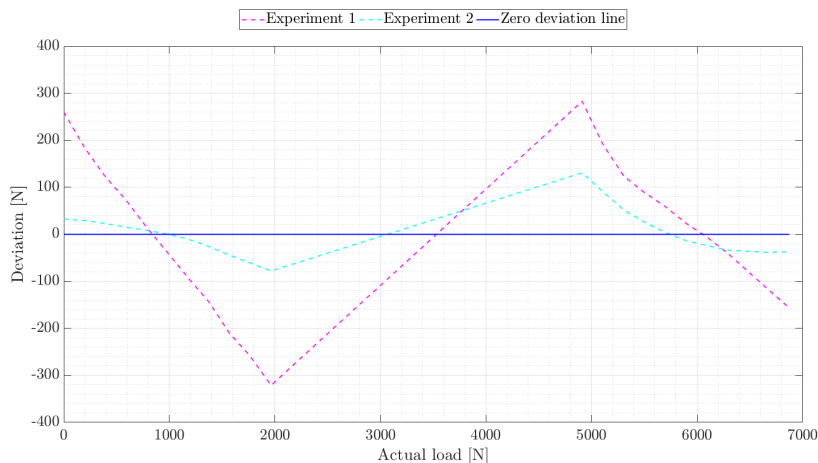


**Figure 4.23:** Deviation between the modelled and actual load for the 18mm and 2mm wall thicknesses.

### 4.3 Comparing the experiments with the numerical analysis

When doing simulations such as the ones in this Master's thesis, the model is assumed to be perfect. For a real life scenario, this is not the case. During manufacturing or other machining of the part, internal stresses may have occurred. This means that the real life case might behave differently than the simulation. This section therefore compares the simulated and real life cases to see how well the simulation fits.

Tables 4.4 and 4.5 compare the simulated and real life cases for the  $2\text{mm}$  and  $18\text{mm}$  wall thicknesses, respectively. The cases are compared at three loads,  $200\text{kg}$ ,  $500\text{kg}$  and  $700\text{kg}$ , which have been multiplied by the local gravitational acceleration at VKL ( $g = 9.82146516$ ) to find the force applied. To calculate the strain from the experiments, equation (2.7) has been used.

The tables show that the simulated and real life cases give strain values of the same magnitude for all the tested cases. For the  $18\text{mm}$  wall thickness, the simulated and measured strain values are very similar, but for the  $2\text{mm}$  wall thickness there is slightly more variation. For a load of  $700\text{kg}$  for example, the difference in strain value is approximately  $9\mu\text{strain}$  for the  $2\text{mm}$  case. As the experiment gave a value of  $16\mu\text{strain}$ , the difference is more than 50% of the measured value.

The findings here indicate that the simulated model will give a good indication of the magnitude of the strain, but not necessarily the correct value. As the  $18\text{mm}$  case gave a more accurate result than the  $2\text{mm}$  case, it can likely be assumed that a thinner wall thickness, and therefore also a more sensitive system, will give greater deviations between the simulated and real life scenario. The simulations should however give a good indication of how good a signal the strain gauges will get.

**Table 4.4:** Comparing the simulations to the experiments for the  $2\text{mm}$  wall thickness.

Load (kg)	Force (N)	Simulated stress (MPa)	Simulated strain (mm/mm)	Measured strain in experiment (mm/mm)
200	1964	6.8679	$7.133 \times 10^{-6}$	$5.2 \times 10^{-6}$
500	4911	17.173	$1.7836 \times 10^{-5}$	$1.23 \times 10^{-5}$
700	6875	24.041	$2.4967 \times 10^{-5}$	$1.6 \times 10^{-5}$

**Table 4.5:** Comparing the simulations to the experiments for the  $18\text{mm}$  wall thickness.

Load (kg)	Force (N)	Simulated stress (MPa)	Simulated strain (mm/mm)	Measured strain in experiment (mm/mm)
200	1964	1.8137	$1.5021 \times 10^{-6}$	$1 \times 10^{-6}$
500	4911	4.5353	$3.7564 \times 10^{-6}$	$3.97 \times 10^{-6}$
700	6875	6.349	$5.2574 \times 10^{-6}$	$5.8 \times 10^{-6}$

## Conclusion

In this Master's thesis, a system for measuring the axial load on a Francis turbine test rig has been tested. Strain gauges have been placed on the lower part of the bearing block, with the aim of having them measure the axial force in the turbine when the turbine is running. The need for measuring the axial force when the turbine is running, is to know that the axial bearing is dimensioned correctly.

Experiments have been conducted in the Waterpower Laboratory, using a smaller section of the bearing block named the Axial Load Measuring Device (ALMD). Semiconductor strain gauges were placed in a Wheatstone bridge configuration on the ALMD, and the ALMD was placed in a rig that made it possible to apply an axial force. The ALMD was tested for axial loads between  $0kg - 700kg$ , as the maximum axial force in the turbine was calculated to be  $7000N$ . Experiments were conducted for an  $18mm$  and a  $2mm$  wall thickness. It was found that the strain gauges were very sensitive to temperature change, and a temperature compensation was therefore implemented for the  $18mm$  wall thickness. A numerical analysis using Ansys Mechanical was also set up.

The experiments showed that a thinner wall thickness was better for getting a more accurate calibration curve. For the  $18mm$  wall thickness, the calibration curve deviated a lot from the actual load at times, giving very incorrect values here. The  $2mm$  case also gave some deviation, however much smaller.

Both experiments gave large uncertainties for some of the loads measured. At a load of  $20kg$ , the  $18mm$  case gave an uncertainty of 15% and the  $2mm$  case gave an uncertainty of 36%. These were however the highest errors found for both cases, and the errors decreased for increasing loads, ending up around 1% – 3% for a  $700kg$  load. In general, the  $18mm$  case gave a smaller error than the  $2mm$  case.

The biggest contributor to the error was the hysteresis. For the loads between  $500kg - 700kg$  especially, the hysteresis was predominant. The  $2mm$  case had a large zero deviation, contributing a lot to the total error, which may be the reason why the total error was generally higher for this wall thickness. For both cases the repeatability was good.

When comparing the results from the experiments and the simulation in Ansys Mechanical, it was found that the simulations gave strain values within the same order of

magnitude, but not the same precise value as the experiments. The simulations correlated more with the  $18mm$  wall thickness than with the  $2mm$  wall thickness.

This Master's thesis has showed that when using strain gauges to measure the axial load for a  $2mm$  and  $18mm$  wall thickness, the uncertainty can be large. If the axial bearing is dimensioned for such a large uncertainty, this system can be used to measure the axial force on a Francis turbine test rig. It is however advisable to reduce this error. Even though the uncertainty was greater for the  $2mm$  wall thickness, this gave a more correct calibration curve, and should therefore be the basis for further development.



## Further work

This Master's thesis concluded that the  $2\text{mm}$  wall thickness should be the basis for further development. The uncertainty was however large for some measuring point, among others at BEP, and further work should therefore be done to finish the development of the axial load measuring system.

To make the uncertainty smaller, a thinner wall thickness should be tested. The numerical analysis showed that a wall thickness of  $1\text{mm}$  was possible without having the material yield, and this should therefore be tested.

A temperature compensation was not conducted for the  $2\text{mm}$  wall thickness due to lack of time. It is recommended that this is done.

When machining the  $2\text{mm}$  wall thickness, the whole inside of the ALMD was removed. To keep the bearing block from leaking, there needs to be an O-ring. A final design where the necessary features are in place therefore needs to be made.

The idea was also to use the ALMD to measure the friction torque at TTL. No work has been done on this topic in this Master's thesis, and should therefore be done in the future. A rig that can apply a torque should be set up and the torque should be measured with strain gauges. As the friction torque is assumed to be small, the ALMD should be weakened in the moment direction. An idea is to take out strips of material from the ALMD, weakening it in the moment direction, but to leave parts of the ALMD thicker to make it strong in the axial direction.



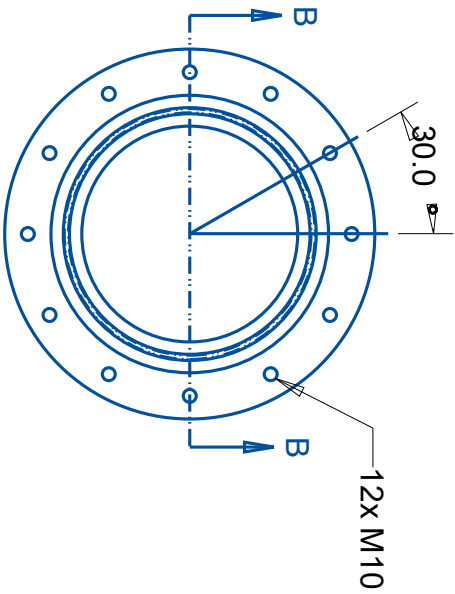
# Bibliography

- [1] FN-sambandet, *Nepal*. [Online]. Available: <https://www.fn.no/Land/Nepal>.
- [2] USAID, *South Asia Regional Initiative for Energy*, 2011. [Online]. Available: [https://web.archive.org/web/20120425173323/http://sari-energy.org/PageFiles/Countries/Nepal\\_Energy\\_detail.asp](https://web.archive.org/web/20120425173323/http://sari-energy.org/PageFiles/Countries/Nepal_Energy_detail.asp).
- [3] B. Thapa and O. G. Dahlhaug, "Turbine Testing Laboratory and its Role in Hydropower Development," 2009.
- [4] *Second Anniversary Issue - Turbine Testing Lab*, 2013.
- [5] Bidhan R. Halwai, *Design of a Francis turbine test rig - Project Thesis*, 2012.
- [6] Johanne Seierstad, *Design system for primary calibration of flow*, 2013.
- [7] Inger Johanne Rasmussen, *Design of a Francis model test rig at Kathmandu University*, 2013.
- [8] Magomed Selmurzaev, *Design of the measurement setup for the friction torque and axial load on the Francis turbine test rig*, 2016.
- [9] Morten Grefstad, *Development of a Francis Turbine Test Rig at Kathmandu University*, 2017.
- [10] Andreas Kjerschow, *Development of a Francis Turbine Test Rig at Kathmandu University*, 2017.
- [11] Julia Bådsvik, *Development of a Francis Turbine Test Rig at Kathmandu University - Project Thesis*, 2018.
- [12] Bård Brandåstrø, *The Waterpower Laboratory at NTNU - A brief Introduction to the Laboratory*. Vannkraftlaboratoriet NTNU, 2002.
- [13] Hermod Brekke, *Grunnkurs i hydrauliske strømningsmaskiner*. Vannkraftlaboratoriet, NTNU, 2000.
- [14] Mechanical Booster, *Francis Turbine Working Principle, Main parts, Diagram and Application*. [Online]. Available: <http://www.mechanicalbooster.com/2018/01/francis-turbine.html>.

- [15] International Electrotechnical Commission, *IEC 60193 Hydraulic turbines, storage pumps and pump-turbines - Model acceptance tests*. IEC, 1999.
- [16] O. A. Olsen, *Instrumenterings teknikk*. Tapir, 1989.
- [17] “Strain Gauge Measurement-A Tutorial,” Tech. Rep., 1998. [Online]. Available: [http://elektron.pol.lublin.pl/elekp/ap\\_notes/NI\\_AN078\\_Strain\\_Gauge\\_Meas.pdf](http://elektron.pol.lublin.pl/elekp/ap_notes/NI_AN078_Strain_Gauge_Meas.pdf).
- [18] K. Hoffmann, *An Introduction to Measurements using Strain Gauges*. Hottinger Baldwin Messtechnik GmbH, 1989.
- [19] Hermod Brekke, *Pumper & Turbiner*, 2003.
- [20] Ole Gunnar Dahlhaug, “Hydraulic axial forces in a Francis turbine.”
- [21] Pål-Tore Storli, “Introduction to turbo machinery.”
- [22] VKL staff and students, “Procedures for the Francis Turbine Test Rig.”
- [23] Jarle Johannessen, *Tekniske tabeller*. Cappelen, 2002.
- [24] Kulite, *Strain Gage Manual*, 2011.
- [25] Deutscher Kalibrierdienst, *Guideline DKD-R 6-1 Calibration of Pressure Gauges*, 2003.
- [26] K. Hoffmann, *Applying the Wheatstone Bridge Circuit*.

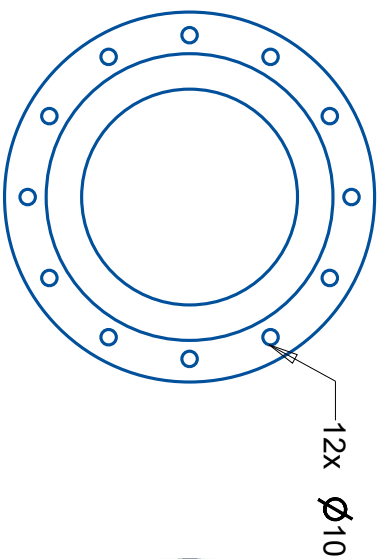
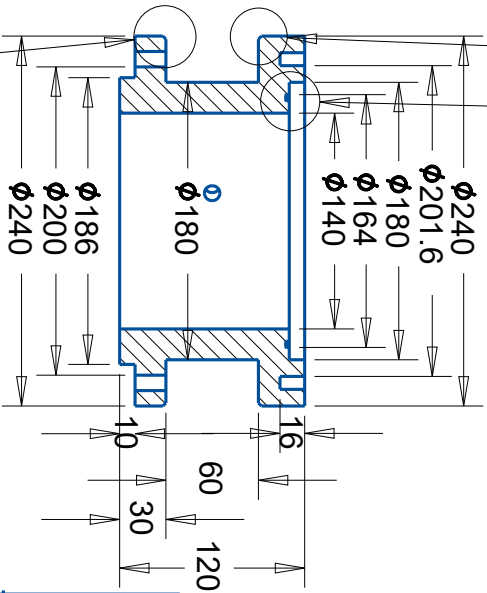
Appendix **A**

# Machine drawing of the ALMD



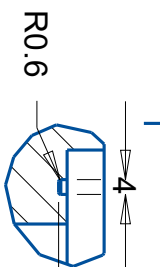
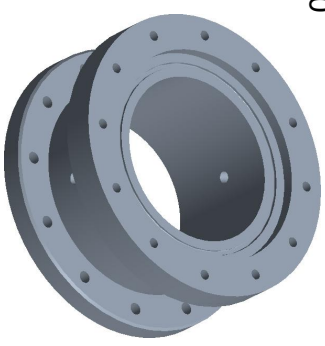
TOP VIEW

SEE DETAIL A  
SEE DETAIL B

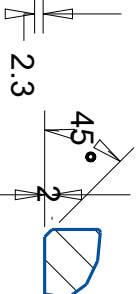


BOTTOM VIEW

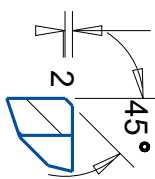
SCALE 0.200



SCALE 0.600



SCALE 0.600



SCALE 0.600

NTNU

Scale: 0.25

Axial load part for TTL Francis turbine

# Appendix **B**

## Procedure for conducting temperature compensation with strain gauges

### Abbreviations and definitions

Symbol	Quantity	Unit
$T$	Temperature	$^{\circ}C$
$a_1, a_2, a_3, a_4, a_5$	Equation parameters	—

### Setup

Four strain gauges are mounted on the Axial Load Measuring Device (ALMD) in a Wheatstone bridge, where the signal from the strain gauges goes through a DAQ-unit to a computer. The ALMD is placed in a heating cabinet. A temperature probe is in contact with the metal, and insulated from the air temperature using insulation.

Both the signal from the strain gauges and temperature are logged using a LabVIEW program. Figure (B.1) shows the setup.

## **Equipment**

- The ALMD
- Strain gauges
- Temperature probe
- DAQ-unit
- Computer

## **Calibration**

### **1. Preparation**

- Place the ALMD in the center of heating cabinet so that the strain gauges are equally influenced by the change in temperature.
- Take the wires outside the heating cabinet and connect them to the DAQ-unit.
- Place a temperature probe on the inside of the ALMD so that it is in contact with the metal. Keep it from the air temperature using insulation.
- Close the door and set the temperature to a maximum temperature. The maximum temperature is decided based on the likely maximum temperature the ALMD will experience when the Francis turbine test rig is in operation.

### **2. Calibration**

- Start heating the heating cabinet.
- Start logging the output from the strain gauges and temperature probe.
- Let the logging continue until the temperature has stabilized at the maximum temperature.

### **3. After the measurements**

- Turn off the logging.
- Turn off the heating cabinet.
- Turn on the logging again, this time logging to a different file and record the cooling of the ALMD.
- Open the door to the heating cabinet to let the ALMD cool down.

Repeat this sequence several times to get several measurements. Record to different files every time.



## Computations

Use the data acquired in the measurements to find a best fit curve between all the temperature curves. Use the lowest order of polynomial that gives a good result. Here, a fourth order polynomial has been used, where  $a_1, a_2, a_3, a_4$  and  $a_5$  are constants given by the best fit curve.

$$y = a_1 \cdot T^4 + a_2 \cdot T^3 + a_3 \cdot T^2 + a_4 \cdot T + a_5$$

Use the polynomial above and subtract it from the measurements when the Francis turbine test rig is run. The axial force should then be compensated for temperature.



**Figure B.1:** The ALMD placed in the heating cabinet.

# Calibration procedure for the Axial Load Measuring Device

## Abbreviations and definitions

Symbol	Quantity	Unit
$F$	Force	$N$
$a_1, a_2, a_3$	Equation parameters	–
$c$	Strain gauge reading	$mV/V$

## Setup

The Axial Load Measuring Device (ALMD) is fastened to a flat plate that rests on two support beams. A coverplate is fastened to the lower flange, which has a hole in the middle. In the hole a ring is fastened. A pulley device is fastened to the ring, and the load can be hung from the other end of the pulley. A weight dish is used to place the weights on. The setup can be seen in Figures (C.1) and (C.2).

The calibration follows the measuring sequence found in Figure (C.3). Weights are added incrementally between  $0kg - 700kg$ , as the maximum axial force has been calculated to be  $7000N$  at TTL. Strain gauges are used to measure the load and their signal is sent through a DAQ-unit to a logging program in LabVIEW. The temperature is also recorded during the calibration in order to be able to compensate for temperature.

## Equipment

- Calibrated weights
- The ALMD
- Strain gauges
- Temperature probe
- A rig to apply an axial force
- DAQ-unit
- Computer

## Calibration

### 1. Preparation

- Put on necessary personal protective equipment, including safety shoes and gloves.
- Place the ALMD in the rig. Fasten it in the upper flat plate with all the twelve bolts. Fasten the coverplate on the lower flange with the ring fastened in the hole. Place the pulley in the ring and hang a weighing dish from the pulley so that it is hanging in mid air.
- Connect the strain gauges to the DAQ-unit and the DAQ-unit to the LabVIEW program.
- Place a temperature probe on the metal and insulate it from the air temperature using insulation. Connect it to the DAQ-unit so that the LabVIEW program can read it.
- Seal off the area around the rig and stop access to any other locations where human activity may disturb the calibration. The strain gauges are very sensitive, and will detect even small vibrations such as people walking.

### 2. Calibration

- Follow the measuring sequence shown in Figure (C.3). Start with three maximum and minimum loads before adding loads incrementally between  $0kg - 700kg$ .
- Start each measurement after a new load has been added. The system should be given the same amount of time to stabilize between every incremental load added.

### 3. After the measurements

- Lower the weight dish to the ground so that it is in a safe position.
- Clear away all the equipment used.

## Computations

From the measurements recorded with the calibrated weights, a calibration curve can be found. A best fit curve is plotted between the data points after the loads have been multiplied by the local gravitational acceleration. The force is then given by a second order polynomial as seen in the equation below.  $a_1$ ,  $a_2$  and  $a_3$  are constants given by the best fit curve.

$$F = a_1 \cdot c^2 + a_2 \cdot c + a_3$$

The strain gauges are very sensitive to temperature, and a temperature compensation should therefore be performed. See *Procedure for conducting temperature compensation with strain gauges* for a procedure to do this.

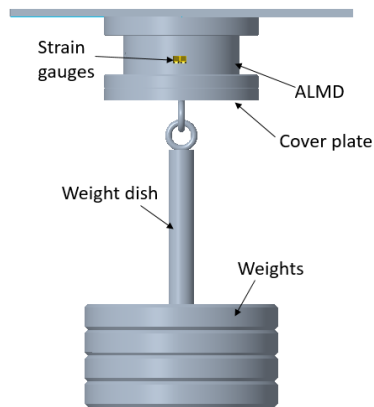


**Figure C.1:** Illustration of the setup of the axial load rig.



**Figure C.2:** The calibration of the ALMD.

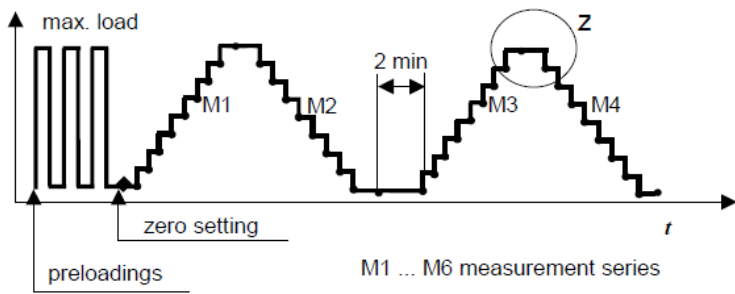


**Figure C.3:** Measuring sequence. [25]